Pile Design Using Wave Equation Analysis Program Application in Offshore Wind Farm

by

Siddharth Chauhan

BTech, Indian Institute of Technology Bombay
Mumbai, India
(2007)

Submitted to the Department of Civil and Environmental Engineering
in partial fulfillment of the requirements for the degree of

MASTER OF ENGINEERING
in Civil and Environmental Engineering

at the

MASSACHUSETTS INSTITUTE OF TECHNOLOGY

June, 2008

Signature of Author: _____
Department of Civil and Environmental Engineering
May 23, 2008

Certified by: _____
Dr. Andrew J. Whittle
Thesis Supervisor

Accepted by: _____
Professor Daniele Veneziano
Chairman, Departmental Committee for Graduate Students

Pile Design Using Wave Equation Analysis Program Application in Offshore Wind Farm

by

Siddharth Chauhan

Submitted to the Department of Civil and Environmental Engineering on May 9, 2008 in partial fulfillment of the requirements for the Degree of Master of Engineering in Civil and Environmental Engineering.

Abstract

Pile driving has been of interest to geotechnical engineers for a very long time. Originally, empirical pile driving formulae were used to interpret pile displacements caused by a hammer blow. Smith (1960) proposed a numerical solution for wave propagation in an elastic pile using a finite difference scheme, with lumped mass representation and simple rheological laws for pile-soil interaction. Since then, many significant parameters affecting pile driving have been included in the wave equation analysis. The offshore industry finds much application of pile driving analysis, especially after recent developments in instrumentation and electronic computational tools. Positioning of wind farms offshore and designing a foundation for a floating platform is a challenge to geotechnical engineers. One of the methods to anchor the floating platform is to tether it down to the seabed with help of driven piles. This thesis considers a typical offshore site for designing a driven pile for floating wind farm. The Author has carried out a set of numerical simulations to analyze pile driving at this site using a commercial program (GRLWEAP), and illustrates how this program can be used in pile design.

Thesis Supervisor: Dr. Andrew J. Whittle

Title: Professor of Civil and Environmental Engineering

Acknowledgments

I take this opportunity to thank the following people who have influenced this report in some way:

Professor Andrew J. Whittle for his valuable guidance and support throughout the development of this thesis. I sincerely appreciate his efforts to make weekly meetings possible, each of which was a very good learning experience for me. I also want to thank him for his permission to use figures from Course 1.364 notes in this thesis.

Professor Deepankar Choudhury, who was my undergraduate thesis advisor at IIT Bombay, for motivating me to pursue graduate studies.

MEng '08 students, who were a source of inspiration and moral support for me. I learnt a lot from some of them and it was a great year.

My parents, for their unconditional love and blessings and my brother, for always being there for me.

List of Figures

List of Tables

Page Number

TABLE OF CONTENTS

1. Introduction

This thesis describes an approach to the design of driven pile foundations for an offshore floating wind turbine system. There has been a ten-fold reduction in cost of on-shore wind energy technology in many areas of United States in the past two decades (Musial et al., 2006). Onshore wind energy development was initially focused on windiest sites with Class 6 winds (average speed of 7.4 m/s at 10 m above surface) and hence, concentrated on remote areas in the western US. Efforts are being made to reduce the cost of onshore wind energy and integrate it into the electric utility grid. However, wind resources over the ocean are also considered to take advantage of full domestic wind electric potential. Some preliminary studies done by the National Renewable Energy Laboratory (NREL) suggest that the offshore source is greater than 1000 GW for the United States (Musial and Butterfield, 2004). According to preliminary analysis of US Department of Energy, a concerted research and development effort to develop offshore wind energy can result in an installed offshore wind energy capacity of 50 GW in the US in the next 20 years representing approximately 5% of the nation's current electric generating capacity (Musial et al., 2006). At current pricing, it will require an investment of $100 billion with at least half of it going to offshore design and construction contracts.

Offshore wind energy can compete other sources of energy in highly populated coastal areas where onshore wind energy in generally not available. The first offshore wind turbine was installed in Sweden in 1990 with a single 300 kW turbine, but the industry has grown very slowly after that. Until 2006, there were 18 operating projects with an

installed capacity of 804 MW (see Figure 1.1 for the breakdown of this capacity as a percentage of the total capacity and by country). Appendix A summarizes the specifications of some offshore wind farm projects. New offshore wind energy projects with capacity of over 11 GW are planned before year 2010, at least 600 MW of which were in permitting process until 2005 in the US (http://www.offshorewindenergy.org/). All the installations are in shallow waters with depths less than 18 m and distances from shore range from 1-14 km. The largest turbine to date installed offshore is in the Irish Sea with an output capacity of 3.6 MW and weighing about 290 metric tons.

Monopiles have been used in shallow depths because they have minimal design development requirements for transition from onshore to offshore environments and they have minimal footprint on the seabed, for example, the wind farm at Horns Rev off the west coast of Denmark (http://www.hornsrev.dk/). The problem with monopiles is that they are flexible and hence depth-limited. This means that the natural frequency of the turbine/support structure system matches the excitation frequency of waves at greater depths and makes the foundation unstable. The monopile length, diameter and thickness will have to be increased with depth to maintain adequate stiffness, which will increase the costs and require specialized and expensive equipment, such as pile hammers. These limits lie somewhere between 20-30 m (Mohamed, 2004).

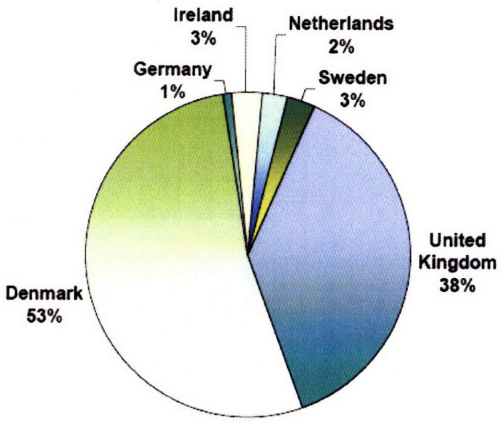

Figure 1.1 Offshore wind energy projects installed up to 2005 (Musial et al., 2006)

The other type of foundation system used for offshore wind turbine is a gravity base foundation, which has been successfully used at the Nysted project in southeastern Zeeland in Denmark having a capacity of 160 MW, and at Samsoe in northeastern Jutland in Denmark. These foundations do not have flexibility issues but their costs increase rapidly with water depth (Musial et al., 2006). However, use of concrete for such foundations can provide some advantage as far as economic feasibility is concerned (Volund, 2005). They also require extensive site-specific soil analysis to assure homogeneous soil properties, compaction to minimize uneven settling and significant seabed preparation. But once seabed is prepared, efforts to install them are reduced (Wind Directions Gravity Foundations, 2003). A lot of research is being carried out for the development of suction bucket foundations, which can be used in shallow water sites without the need for pile driving (Isben, 2005) (see Figure 1.2).

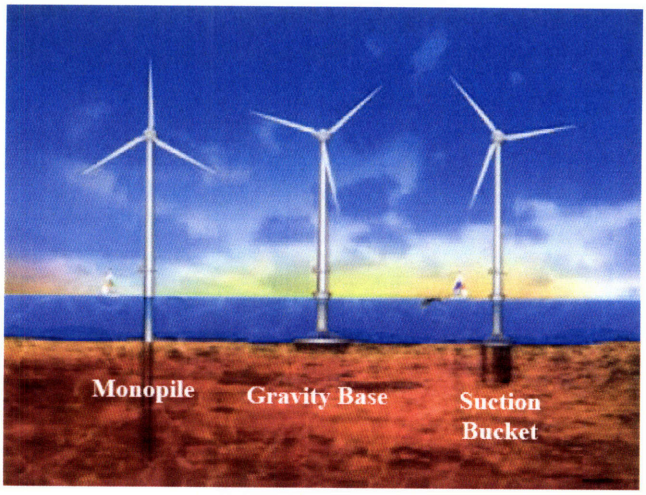

Figure 1.2 Foundations in shallow waters (Musial et al., 2006)

The current practice of driving monopiles into the sea bed or relying on concrete gravity bases for fixed-bottom offshore wind turbines is not economically feasible in deep waters (water depths greater than 30 m) (Jonkman and Sclavounos, 2006) because a significant part of the total cost of an offshore wind farm comes from the foundation system (see Figure 1.3). Hence, emphasis is being placed on floating offshore wind turbine support platforms, as they may be the most economical means of installing offshore wind turbines (Jonkman and Sclavounos, 2006).

The winds blowing over sea are faster and more uniform than on land. The environmental states representing a range from *light* to *severe* weather conditions have mean wind speed of 2.5 – 20 m/s in fully developed seas with significant wave heights of 0.09 – 13.72 m, respectively (Lee, 2004). These strong winds increase the potential of energy that can be tapped by offshore wind turbines, but at the same time, they are the source of large overturning moments for the whole structure. Figure 1.4 shows the six standard modes of motion that are considered in wave-body interaction theory. Modes 1-3 are the

translational modes of surge, sway and heave and modes 4-6 are the rotational modes of roll, pitch and yaw. "U" denotes the load due to wind, which generates moment about the origin of the coordinate system shown.

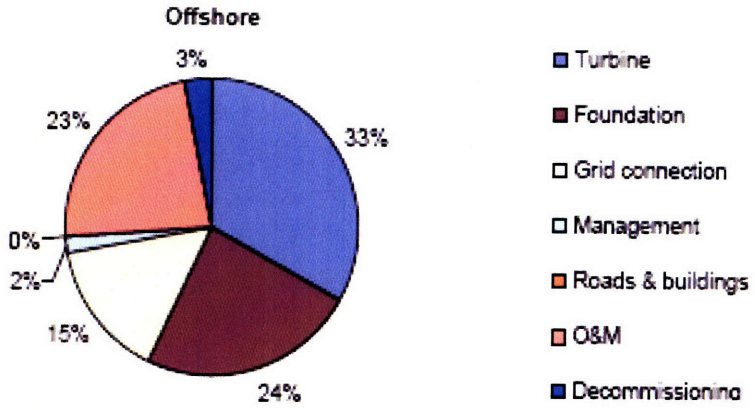

Figure 1.3 Typical break-up of cost for an offshore wind farm (Kuhn et al., 1998)

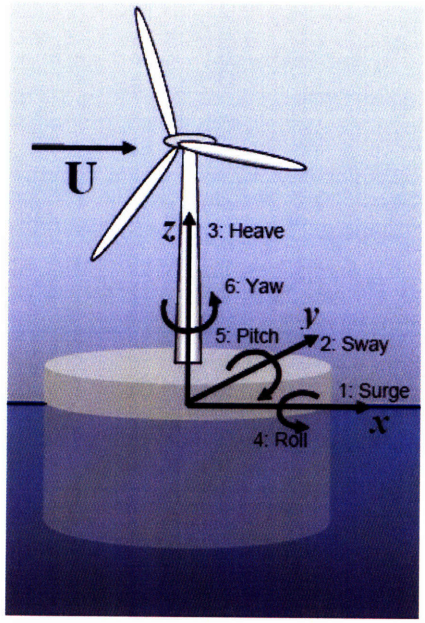

Figure 1.4 Modes of motion of turbine/support structure system (Wayman et al., 2006)

There are three ways to moor the floating turbine:

1. Tension leg mooring systems with vertical mooring lines under tension providing large restoring moments in pitch and roll
2. Slack catenary mooring system providing a base station for an offshore structure with little stiffness
3. Taut catenary system providing more stiffness by increasing the tension in the mooring cables.

When dynamic wave forces act at the bottom of the floating platform, large buoyant forces increase the tension in the tethers, which attach the platform to the seabed. In the case of a Tension Leg Platform (TLP), the tethers must provide adequate restoring in surge to sufficiently limit the steady state offset in surge. The tension in the windward tether must never exceed the maximum allowable tension, and the leeward tether must never go slack or fall below the minimum allowable tension at any point during operation. The total force exerted by the tethers should be enough to counteract the buoyant force acting on the platform for its stability. Figure 1.5 is a pictorial representation of the wind force acting on the turbine and the tower supporting it, and the forces acting on the platform along with vertical and horizontal components of tension in the tether. Wind load is assumed to be uniform with height.

This report considers NREL 5 MW wind turbine because it is speculated that 5 MW is the minimum power rating at which deepwater offshore wind energy can be cost effective (Wayman, 2006). Its general properties are shown in Table 1.1. The performance of the

turbine has been calculated by extrapolating from the performance of smaller wind turbines.

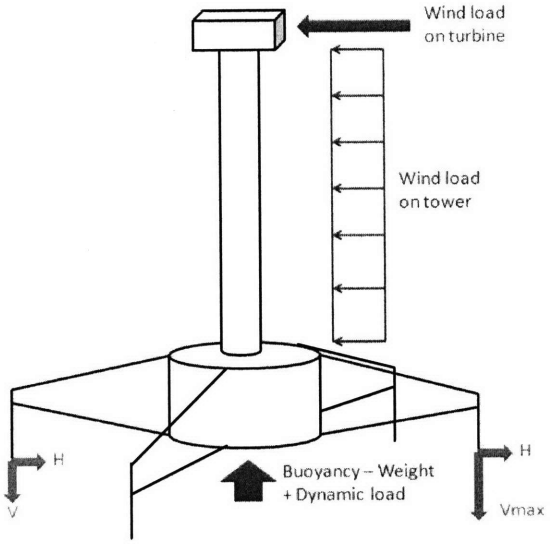

Figure 1.5 Forces acting on the turbine, platform and tethers

The power curve shown in Figure 1.6 (Tracy, 2007) can be used to characterize a wind turbine and wind speeds. Region 1 refers to wind speeds that are too low for the wind turbine to operate and is not shown in Figure 1.6. Region 2 begins at a cut-in speed of 3 m/s at which the turbine begins to operate and its power increases with speed. The highest wind speed in region 2 is the speed at which the turbine generates power for which it is rated. In region 3, as the wind speed increases the wind turbine maintains a constant power by adjusting the pitch angle of the blades to allow for power to pass by. The highest speed in region 3 is the speed beyond which the turbine completely feathers its blades to protect the wind turbine during extreme winds.

Table 1.1 Gross properties of the NREL 5 MW Offshore Wind Turbine (Wayman, 2006)

Rotor Orientation	Upwind
Control	Variable Speed
Rotor Diameter/Hub Diameter	126 m/3 m
Hub Height	90 m
Max Rotor/Generator Speed	12.1 rpm/1173.7 rpm
Maximum Tip Speed	80 m/s
Overhang/Shaft Tilt/Precone	5 m/5^0/-2.5^0
Rotor Mass	110,000 kg
Nacelle Mass	240,000 kg
Tower Mass	347,460 kg

The design constants and structural properties of the platform considered by Tracy (2007) are summarized in Table 1.2. The corresponding maximum tension in the tether for six meter sea state* is found to be 783 metric tons. This value of tension in the tether has been taken as maximum uplift load for designing driven piles. The design load is therefore, 2350 metric tons considering a factor of safety of 3. It should be noted that since the load applied by the tethers on the pile is vertically upwards, all the capacity of the pile must come from shaft friction.

This report, therefore, has two objectives:

- To design driven piles for an offshore floating platform for wind turbine, using wave equation analysis approach,
- To recommend equipment for driving pile.

* Six meter sea state means that the average height of the one-third highest waves is six meters

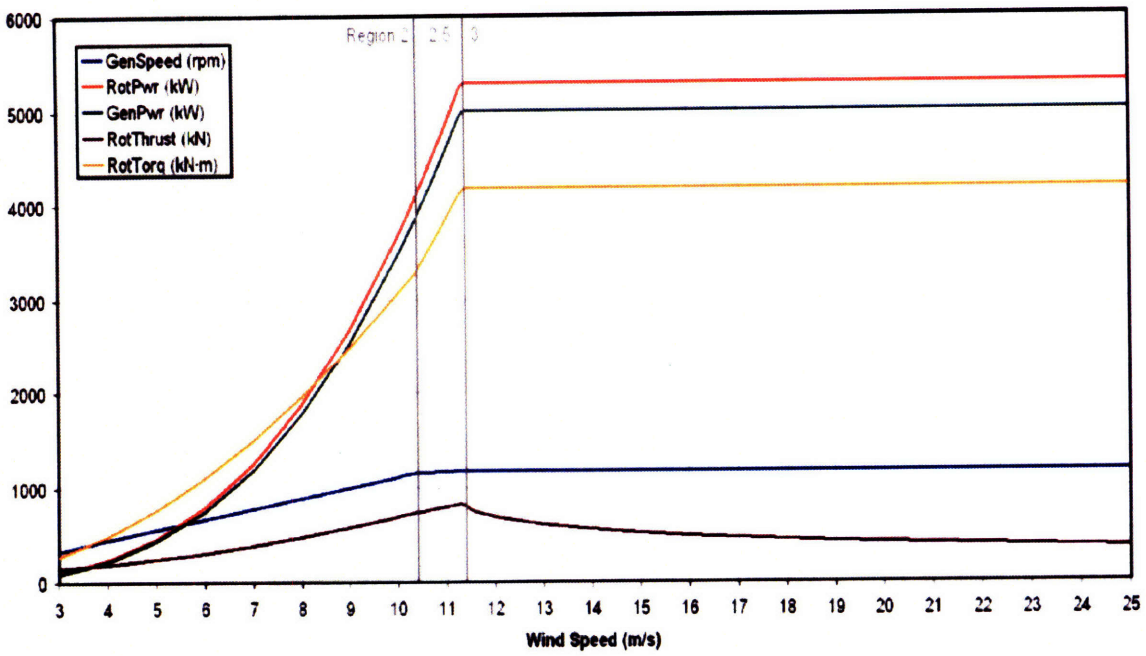

GenSpeed	Angular speed of the high-speed shaft and generator
RotPwr	Mechanical rotor power
GenPwr	Electrical generator power
RotThrust	Rotor thrust

Figure 1.6 Performance regimes of the NREL 5 MW wind turbine (Wayman, 2006)

Table 1.2 Design constants and structural properties of the platform (Wayman, 2006)

Constant	**Value**
Wind Speed	11 m/s
Turbine thrust	800 kN
Turbine Moment	72,000 kN-m
Freeboard	5 m
Property	**Value**
Steel Mass	326 metric tons
Concrete Mass	5249 metric tons
Steady State Heave Force	3870 metric tons

Chapter 2 discusses the constructability issues in an offshore project. The processes involved in construction of foundation for a floating offshore structure are described focusing on the use of tubular steel piles. The author explains the steps in design, fabrication, transportation and installation of the pile. Chapter 3 explores some methods of pile driving analysis and focuses on analysis by wave equation. It reviews the wave equation analysis first proposed by Smith (1960) and discusses some computational tools based on this formulation. The author has worked with a commercial program GRLWEAP and demonstrates the utility of this program in the solution of standard problem of pile driving (Simons and Randolph, 1984). Chapter 4 provides a detailed analysis of the design process and driving equipment used in this report. A soil profile from the database of Magnus Foundations (Jardine and Potts, 1992) representing a typical offshore condition from the North Sea has been used as a reference profile for example calculations. The author describes the selection of parameters for this sample profile. Chapter 5 is conclusion of the thesis.

2. Pile Installation

An offshore wind farm requires a close integration between design and construction because of the challenges of operating at sea. The installation of an offshore structure consists of transporting the various components of the structure to the installation site, assembling and positioning the various components into a stable structure in accordance with the design (API RP 2A, 1987). The method of installation of a foundation system for an offshore structure depends on the type of the structure and the seabed conditions. This section of the report focuses on methods of installing tubular steel driven piles for offshore wind farms by discussing some existing offshore wind farms.

Foundation piles can be carried to the installation site on a barge. Typical offshore barges are 80 to 160 m in length (Gerwick, 2007). Width of the barge should be one-third to one-fifth of the length. Depth is typically 1/15 of the length. But in the case of existing offshore wind farms where, large monopiles with diameter up to 4 m, penetration depth of around 33 m and weight of up to 270 Tonnes have been employed, piles have been offloaded directly to the sea and floated to the installation site towed by tugboats (LIC Engineering, 2003) (see Figure 2.1). This can save costs on leasing and/or buying a barge for transporting the piles to the site. But this might not be applicable where multiple piles are used for foundation and the use of a barge may be inevitable.

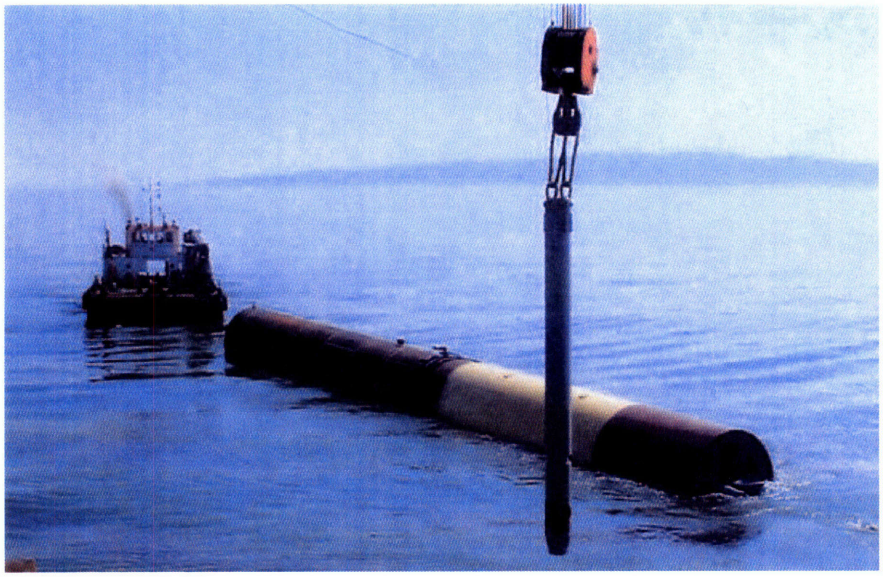

Figure 2.1 A monopile being towed away to the installation site (LIC Engineering, 2003)

Before a pile is installed on the seabed, a "mattress" of rock and stones is placed around the foundation to protect against erosion (scour) (Ciamberano, 2006). This requires scour analysis and prediction of scour development envelopes (LIC Engineering, 2003). It can be done by filling these regions, where scouring can take place, by rock with grading depending on the seabed conditions. A pile can be driven by using a jack-up vessel, or a specially designed barge which can transport, install and maintain assembled wind turbines (one such barge is patented in Netherlands (www.offshorewindenergy.org/)). This requires use of a heavy-duty hammer, which can work underwater (see Appendix C for a list of hammers which can operate underwater). The effects of pile driving accessories on the performance of the driving process are discussed in Appendix D (parametric study).

In the case of Scroby Sands Wind farm (LIC Engineering, 2003), a flange was welded on the top of the steel monopile (see Figure 2.2) and hammer anvil placed directly on it. The pile (diameter of 4.2 m, penetration depth 31 m and weighing up to 210 metric tons) was driven successfully within tolerances and without any damage to the flange in a period less than 24 hours/pile. Figure 2.2 shows the pile top closed with a metal plate, which acted as an internal platform to carry out installation of boat landing and access platform immediately after driving.

Figure 2.2 Monopile used at Scroby Sands Wind farm (LIC Engineering, 2003)

After the pile is driven, a transition piece complete with pre-installed features such as boat landing arrangement, cathodic protection, cable ducts for submarine cables, turbine tower flange, etc. is cast together with the monopile (Ciamberlano, 2006). It is attached to the monopile in a special concrete casting process. Its top rim is a flange that accommodates bolting of the turbine tower and also helps in raising the tower to a completely vertically position even if the foundation is not completely level. The

protective rock mattress may be finished with an additional layer of rock and stones (see Figure 2.3).

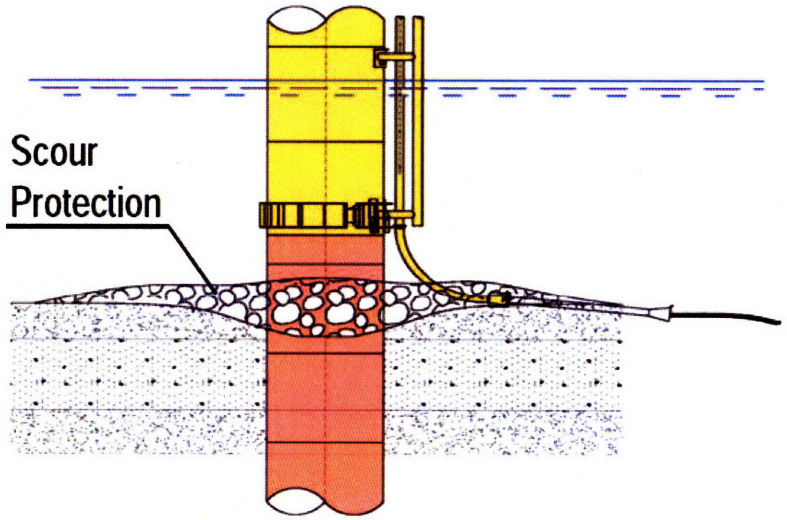

Figure 2.3 Scour protection for a monopile of a wind turbine (LIC Engineering, 2003)

Some existing offshore wind turbines stand on piles installed by core drilling and grouting. For example, Blyth Wind farm (LIC Engineering, 2003) (see Appendix B) with 2 MW turbine installed on a 3.5 m diameter steel monopile with penetration depth between 12 m and 15 m. A pilot hole was drilled through the upper layers to be used for initial centralization during the following drilling of the full bore hole. A large coring drill bit guided by full size conductor casing was used. The hole was slightly oversized and a casing shoe was left in the top of the hole to avoid collapse of the hole in the top section and guide the pile. Then the 150 metric ton heavy pile was lifted by a rig crane and lowered through the casing shoe into the rock socket. Grouting was then done and the access platform bolted at the top of the pile. An example of an offshore wind farm with

piles installed using driving and drilling techniques both, is the North Hoyle Wind farm (LIC Engineering, 2003) (see Appendix B).

Once the piles are installed, the wind turbines can be mounted on the piles either using a jack-up barge or a floating crane vessel (see Figure 2.4) depending on the water depth, the crane capability and the vessel capability (Offshore Wind Energy Workshop, 2003). See Table 2.1 for vessels suitable for turbine installations. The crane must be able to lift the turbine, with hook heights greater than the level of the nacelle so that the tower and turbine can be installed. Specially built vessels like the one patented in Netherlands can save significant amount of time (and hence cost).

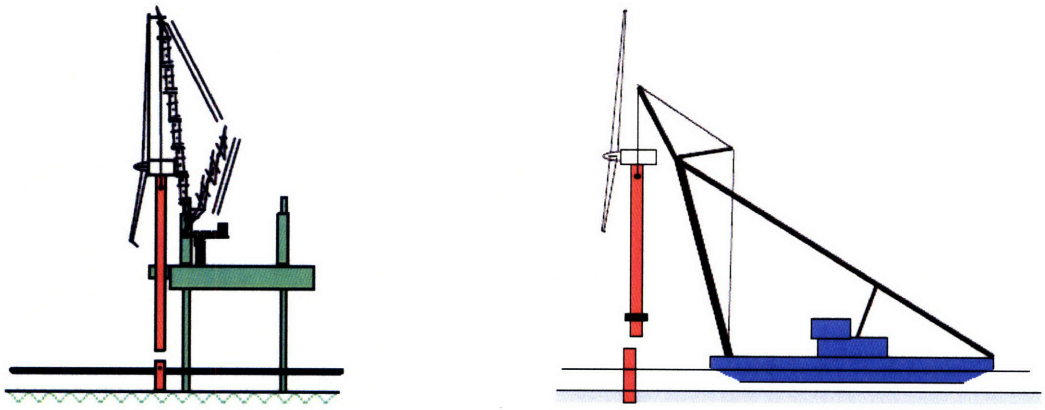

a) Jack-up barge construction b) Floating crane vessel construction

Figure 2.4 Wind turbine installation on the monopile

(Offshore Wind Energy Workshop, 2000)

For a floating wind farm, the pile foundation can be installed in similar way as described above, difference being that the platform carrying the turbine is tethered down to the piles buried in the seabed. The total time to build a multi-unit wind farm is subject to weather

conditions. The installation should be scheduled during calm weather conditions to complete the construction as quickly as possible. This scheduling also depends on the pile setup, which is discussed in Chapter 4 of this thesis.

Table 2.1 Examples of vessels that may be suitable for offshore windfarm installation (Offshore Wind Energy Workshop, 2000)

VESSEL	*VESSEL SIZE*	*GROSS TONNAGE*	*LIFT CAPACITY / HEIGHT*
FLOATING CRANE VESSELS			
Smit Land LM Balder	110m 30m 7.6m	7772t	500t / 60m
Smit Tak Taklift 4	83m 35m 7.0m	4854t	2400t / 75m
Smit Tak Taklift 7	73m 30m 5.5m	3513t	1200t / 65m
Bugsier Thor	76m 24m 4.7m	2667t	350t / 80m
Ugland Uglen	78m 26m 4.3m	1589t	600t / 75m
JACKUP VESSELS with integral crane			
Ballast Nedam Buzzard	43m 30m 4.2m	c1750t	198t / 62m
Interbeton IB909	43m 30m 4.4m	1796t	272t / 57m
Amec Wyslift	38m 32m 4.4m	1410t	280t / 50m
Seacore Deep Diver	30m 20m 4.5m	1675t	50t / 51m

3. Pile Driving Analysis by Wave Equation

3.1 Introduction

The most reliable method to determine the load-carrying capacity of a pile is by a load test but not all of the piles at a site can be tested due to economic reasons (Chow et al., 1987). One of the alternatives adopted to predict the load-carrying capacity of a driven pile is the use of pile driving formulae, which are based on rigid-body mechanics and make use of parameters according to experience in a particular soil type, pile type or driven depth. There was a need to improve upon the erroneous assumptions made in these formulae. It was noted that pile driving is a case of longitudinal impact and governed by wave equation (Isaacs, 1937). Pile driving analyses are generally accomplished by modeling 1-D wave propagation in an elastic rod (pile). The methods routinely used are based on a lumped mass discretization of the pile with simplified rheological models of pile-soil interaction following the framework first proposed by Smith (1960). The Smith (1960) model simulates 1-D wave propagation in the pile, pile cap assembly and hammer system using finite difference scheme as shown in Figure 3.1.

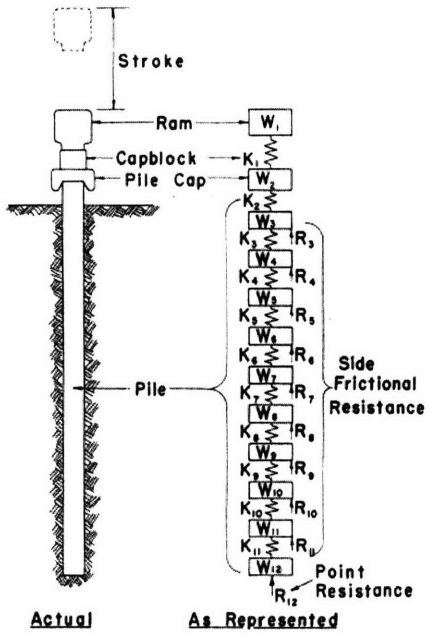

Figure 3.1 Smith's spring model (Smith, 1960)

The time-period during which the force pulse travels along the pile and comes back to the pile head after reflection from the pile tip, should be divided into smaller intervals enough to keep the step-by-step calculations ahead of the stress wave. The smaller the length of the individual pile sections, the smaller must be the time interval. The velocity (and hence the impact) of the hammer produces a displacement in the individual weights. The displacements of two adjacent weights produce a compression or extension in the spring between them. The spring compression or extension produces a force in the spring. The forces of the two springs on an individual weight along with the resistance from ground produces a net force on the weight, which either accelerates or decelerates it. This results in a new velocity and gives a new displacement in the next succeeding time interval. The process is repeated for each weight in each time interval until all downward

velocity is lost. The following equations represent the numerical scheme for wave equation analysis.

$$u(m,t) = u(m,t-\Delta t) + \Delta t\ v(m,t-\Delta t) \tag{3.1}$$

$$C(m,t) = u(m,t) - u(m+1,t) \tag{3.2}$$

$$F(m,t) = C(m,t)\ K(m) \tag{3.3}$$

$$R(m,t) = [u(m,t) - u^p(m,t)]\ K_s(m)[1 + J(m)\ v(m,t-\Delta t)] \tag{3.4}$$

$$v(m,t) = v(m,t-\Delta t) + [F(m-1,t) + M(m)g - F(m,t) - R(m,t)]\frac{\Delta t}{M(m)} \tag{3.5}$$

where, for pile element, m at time t: M is mass, u is displacement, v is velocity; for internal spring, m, at time, t: c is compression, K is stiffness, F is force; for external soil spring, m at time, t: R is soil resistance, K_s is stiffness, J is damping, u^p is irrecoverable deformation/slip = (u-Q), where Q is the 'quake', Δt is the time interval and is equal to $\Delta L/c$, where c is the velocity of the wave propagating in the pile.

The total resistance to driving consists of static soil resistance and a dynamic component to represent damping of the soil. The approximation used in that approach by replacement of the soil continuum by viscous soil springs characterized by non-standard soil parameters, such as the quake value, Q, and viscous damping coefficient, J, and the inability to measure these empirical coefficients directly in a new environment is a major disadvantage of the model (Chow et al., 1988 and Nguyen et al., 1988). It also creates problems such as inaccurate calculations of the stress waveform (Sakai, 1988).

After Smith's (1960) model, some other soil models were proposed. One such model was prepared in the Texas Transport Institute (TTI) (Samson, 1962), which accounted for the non-linearity of the soil damping force with penetration velocity (Chow et al., 1987). The total soil resistance, R_d, in the program developed at TTI is given by the following equation:

$$R_d = R_s(1 + Jv^N) \tag{3.6}$$

where R_s is the spring component of soil resistance, J is the damping coefficient and N is an exponent (N<1) to account for nonlinear relation between damping force and velocity, v, of the pile. Experiments indicate exponents of N = 0.18 for clays and N = 0.20 for sands (Rausche et al., 1992).

Another soil model was proposed by Goble and Rausche (1976) at the Case Western reserve University (CWRU) where the soil damping force was uncoupled from the soil spring force and the total resistance, R_d, during driving was given by

$$R_d = R_s + J_c Z_p v \tag{3.7}$$

where J_c is a dimensionless damping constant (not a soil property) and Z_p is the impedance of the pile defined by $E_p A_p / c_w$; E_p is the Young's modulus of the pile material, A_p is cross-sectional area of the pile and c_w is the longitudinal wave speed given by $\sqrt{E_p/\rho_p}$ where ρ_p is the density of the pile material.

Heerema (1979) suggested a power law to calculate the total soil interface force given by

$$R_t = R_s(a + J_H v^{0.2}) \tag{3.8}$$

where, "a" (dimensionless) and J_H (dimension of $(s/m)^{0.2}$) depend on shear strength of the soil.

The "soil parameters" in the TTI and CWRU computer programs are empirical correlation parameters that have little rational or physical representation (Chow et al., 1987). Randolph and Simons (1986) and Corte and Lepert (1986) proposed improved soil models in which conventional soil parameters are used to characterize radiation damping and spring stiffness (Nguyen et al., 1988). Lee et al. (1988) proposed a model derived from visco-elasto-dynamic theory and the total soil resistance prior to soil failure was given by:

$$R_d = ku + cv \tag{3.9}$$

where k and c are the stiffness and radiation damping coefficients respectively and u is the pile displacement.

A 3-D (axisymmetric) finite element pile-soil model was suggested by Chow and Smith (1984) for the analysis of pile driveability in clays. Standard soil mechanics parameters (Young's Modulus, Poisson's ratio, soil mass density and undrained shear strength) can be used to describe the properties of soil mass and radiation of the stress waves in the soil occurs naturally. One other advantage of this model is that it can be readily adapted to the problem of soil plug in the open-ended pipe piles (Chow and Smith, 1984).

3.2 Dynamic Soil Response

When a pile is driven by an impact hammer, separate blows are given to the pile by raising the hammer either by a rope, compressed gas or air and letting it fall due to gravity. These are called single acting hammer. Double-acting hammers are accelerated downwards to increase the impact energy (Massarsch, 1992). The driving energy is transmitted through a hammer cushion, placed on the head of the pile or in the base of the hammer. Some part of this energy is dissipated in compressing the cushion blocks when driving on the head of the pile. The amount of energy dissipated depends on the stiffness of the cushion and coefficient of restitution (COR) of the cushion material. The energy transmitted (ENTHRU) to the pile generates time-dependent stresses and displacements in the pile. The pile behaves as an elastic bar in which the stresses travel longitudinally as waves with velocity v (see Equation 3.7). The energy transmitted from the pile to the soil through the pile shaft and the toe, depends on the type and efficiency of the hammer, the nature of the impulse (transient or steady-state) and the impedance of the pile (Massarsch, 1992). Both, plastic and elastic deformations occur in the soil due to the pile penetration. Figure 3.2 shows load-deformation characteristics assumed for the soil in Smith's procedure, with path OABC and DEFG representing loading and unloading in side friction.

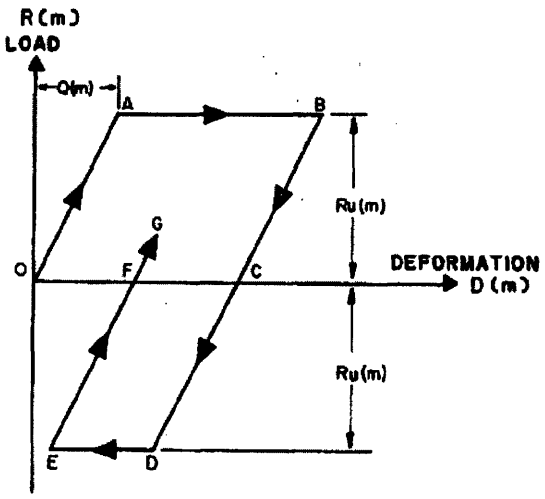

Figure 3.2 Load deformation curve for a soil mass in the spring model

(Texas Transportation Istitute, 1969)

The steady state response of soil around a pile due to axial vibrations of the pile, was studied extensively by Novak (1977) and Novak et al. (1978). The behavior of the pile shaft and tip was analyzed separately. Soil was idealized as a series of independent horizontal layers, as is assumed for load transfer analysis of piles under static loading (Randolph and Simons, 1986). The shear mobilized by an element of pile (radius r_0) subjected to periodic axial vibration $w = w_0 \sin\omega t$ can be written as

$$\tau = \frac{Gw_0}{2\pi r_0}[s_{w1}(a_0)\sin\omega t + s_{w2}(a_0)\cos\omega t] \qquad (3.10)$$

where G is the shear modulus of the soil, and the stiffness coefficients s_{w1} and s_{w2} are functions of the non-dimensional frequency $a_0 = \omega r_0 / v_s$, v_s being the shear wave propagation velocity of in the soil. The soil response is approximated by a simple dashpot in parallel with a spring with the dashpot representing radiation damping. The force mobilized per unit length of the pile shaft is given by

$$T = K_s w + c_s v \tag{3.11}$$

where $K_s = 2.9G$ and $c_s = 2\pi r_0 G/v_s = 2\pi r_0 (G\rho)^{1/2}$ (ρ is the total density of the soil).

The soil reaction to the pile motion at the tip was assumed to be equivalent to the reaction of an elastic half-space to the motion of a rigid circular footing (Simons and Randolph, 1984). A frequency independent spring and dashpot analog, similar to that of interaction along the shaft was obtained by Lysmer and Richart (1966). The coefficients derived for the spring and dashpot were:

$$K = \frac{4Gr_0}{1-\upsilon};\ c = \frac{3.4r_0^2}{1-\upsilon}\sqrt{\rho G} \tag{3.12}$$

where υ is the Poisson's ratio.

Some other methods include energy approach proposed by Paikowsky & Chernauskas (1992) to evaluate capacity of driven piles based on the fact that the total energy transferred to the pile should be equal to the work done by the pile/soil system, and pile capacity prediction using neural networks technique (Dyminsky et al., 2000). These are not discussed further as they are beyond the scope of this thesis.

3.3 Computational Tools for Wave Equation

Stress wave measurements during driving are useful for a better understanding of blow-count curves and give some parameters characterizing the soil resistance. When a hammer strikes the pile head, a longitudinal stress wave is generated in the pile, which propagates downwards with a velocity v (see Equation 3.7). The wave propagates is

partially reflected at the pile tip and soil interface. The stress and velocity measured at the top of the pile are due to the superposition of downward and upward traveling stress waves (Pelleau et al., 1980). These measurements can be made by a combination of acceleration and strain measurements at the top of the pile. These data can converted to velocity and force records respectively, by the *Pile Driving Analyzer®* (PDA) (Rausche, 2000). The PDA can calculate energy transferred to the pile top, pile bearing capacity, pile stresses and other important pile quality parameters using 1-D linear wave equation. It is a user-friendly field data acquisition system and computer that provides power supply, signal conditioning, processing and evaluation of the measured dynamic data (Mukkadam et al., 2000). For details on the electronics and uses of the PDA, one can refer to Likins (1980). The hammer velocity may be obtained using radar technology in the *Hammer Performance Analyzer ™*. A hand held *Saximeter ™* can be used to measure the time gap between two consecutive impacts and calculate the stroke. The instrumentation operation should not cause any delay to the normal driving operation and is to be used in normal offshore driving conditions. The equipment should also be easily transportable to any remote area (Pelleau, 1980).

There are some commercial computer programs available for pile driving analysis by wave equation. One such software is GRLWEAP (Pile Dynamics, Inc., 2005), which has been used by the author in the current analysis.

3.4 GRLWEAP

The GRLWEAP program (Goble et al., 1999) is probably the most widely used wave equation program. It can calculate bearing graphs (ultimate soil resistance vs. blows per unit of distance) and predict the blow count as a function of pile penetration. The driveability analysis for a particular set of driving equipment (such as hammer, cushion, etc.), pile material and dimensions, and a particular type of soil requires a detailed static and dynamic soil resistance input parameters to reflect the various layers that the pile penetrates. From such an analysis, it possible to obtain an estimate of both, the total number of blows required to install the pile, and the total installation time.

Input Parameters

Hammer

For driveability analysis, the user can choose a hammer type from a list of around 700 pre-programmed hammers. The specifications of a hammer, which are provided to the user are the Hammer ID (serial number in the hammer list), the Hammer Manufacturer/Model, Hammer Type (open end diesel, closed end diesel, external combustion hammer or vibratory hammer), stroke, Energy/Power, Ram Length, Ram Diameter, etc. One can choose to create a customized hammer by giving inputs for hammer specification.

Pile

The user can input pile material (steel, concrete or timber), pile length, pile penetration depth, cross-sectional area of the pile, elastic modulus and specific weight of the pile material, toe area and perimeter of the pile. The significance of the toe area input is to model a soil plug in the case of open-ended pipe piles. If the user wants to do the driveability analysis assuming a soil plug, the input value for a specific weight of the pile material changes over the length of the pile where soil plug is assumed to occur according to the following equation given by

$$\rho = (\rho_{soil} A_{plug} / A_{steel}) + \rho_{steel} \tag{3.13}$$

where ρ_{soil} is the specific weight of the soil, ρ_{steel} is the specific weight of pile material (steel), A_{plug} is the cross-sectional area of the soil plug, A_{steel} is the cross-sectional area of the (steel) pile and ρ is the modified specific weight to account for the presence of the soil plug.

Cushion

The user can input cushion cross-sectional area, elastic modulus of cushion material, cushion thickness, coefficient of restitution, cushion stiffness and helmet weight. One can also choose the above input parameters for cushion from a list of in-built parameters.

Soil

The user can specify the soil properties either by soil type-based input form or by SPT-N value based input form. In the soil type-based input form, one can specify the water table depth, number of layers of soils in the soil profile, thickness of each layer and choose a

soil type for the layer (Granular or Cohesive). According to the soil type, values for damping and quake for pile shaft and toe are automatically assigned by the program, based on empirical values used in Smith's model (1960) and reflect accumulated experience of GRL (GRL, 1999) (see Table 3.1).

GRLWEAP Analysis

For a dynamic analysis using GRLWEAP, it is not only necessary to calculate the static resistance and its distribution, but also to estimate dynamic soil resistance parameters, damping and quake, both at shaft and toe. According to GRLWEAP recommendations (GRL, 1999), only the shaft damping is a function of soil type while toe damping is independent of soil type because the dynamic resistance component at the pile toe is more a function of inertia forces caused by the soil being displaced around the pile toe than with forces of viscous flow. Similarly, shaft quake is recommended to be independent of soil type but there exists no evidence if this assumption affects the predictions by the wave equation. Toe quake depends on the pile size at the toe and in the case of rock, the hardness of the material. Table 3.1 summarizes the recommendations by GRLWEAP manual (2005).

Table 3.1 Recommended values for quake and damping factor (GRLWEAP, 2005)

	Soil Type	**Pile Type**	**Q [inch/mm]**
Shaft quake	All soil types	All types	0.1/2.5
Toe quake	All soil types, Soft Rock	Open ended pipes	0.1/2.5
	Dry soils or very danse or hard soils	Displacement piles of ϕ D	D/120
	Submerged soils or loose or soft soils	Displacement piles of ϕ D	D/60
	Hard rock	All types	0.4/10
			Damping Factor J_S [s/ft]/[s/m]
Shaft damping	Non cohesive soils		0.05/0.16
	Cohesive soils		0.2/0.65
Toe damping	In all soil types		0.15/0.5

The static analysis done by GRLWEAP consists of two calculations: the shaft resistance and the toe resistance (Rausche et al., 2000). Shaft resistance is estimated based on an effective stress approach. The unit shaft resistance at a point along the pile is calculated from

$$f_s = K\bar{\sigma}'_v \tan\delta \tag{3.14}$$

where K is the lateral earth pressure coefficient, $\bar{\sigma}'_v$ is the average vertical effective stress, and δ is the friction angle at the soil-pile interface. The effective stress can be calculated by buoyant weight of the soil according to the water table depth specified by the user. The specific weight of the soil and the friction angle are automatically assigned by GRLWEAP based on the soil type (or SPT value in the case of SPT-N value based input form) and cannot be overridden and input manually by the user. The toe resistance in kPa is estimated by using the empirical method proposed by Meyerhof (1976) (GRL, 1999)

$$q_{bf} = \min(200N;\ 12{,}000)\ \text{kPa} \tag{3.15}$$

where N is the SPT N value in the strata at the bottom of the pile. Alternatively, unit shaft and toe resistance values can be calculated using α-method (Randolph and Murphy, 1985) which forms the basis of current API code for design of offshore friction piles in clay, Poulos and Davis (1980) for shaft friction in sands, Skempton's (1951) method for tip resistance in clays, etc. Once the unit shaft resistance and end bearing values are input into the GRLWEAP driveability analysis, toe and shaft damping and quake values assigned according to Table 3.1 (assuming that the user gives the pile effective toe area), the static capacity of the soil is calculated.

The user can also input values for Setup Factor, Limit Distance, and Setup Time. The "Setup Factor" is the ratio of long-term shaft resistance to the static resistance to driving (SRD) along the shaft for a certain soil layer at a certain depth. Pile setup is discussed in more detail in Chapter 4. In GRLWEAP, the setup factor only describes the loss of shaft resistance and does not affect the end bearing. The default value of setup factor is 1.25 for sands, 1.5 for silts and 2.5 for clays. The default value of "Setup Time" in GRLWEAP, the basis of which is unknown to the author, is 1 hour for sands, 1 day for fine sands and silts and 7 days for clays. "Wait Time" accounts for any interruptions during driving. The user can specify depths at which the analysis is to be performed to generate blow count vs. depth graph. For each analysis depth, the total number of blows is calculated by integrating blow counts over depth. The pile driving time is calculated from the total number of blows assuming a blow rate. The calculated driving time does not include any wait times specified at the analyzed depths. Figure 3.3 shows an example of driveability graph generated by GRLWEAP. It shows the computed static capacity of the soil at selected depths and the blow count (blows/ft) necessary to drive the pile at those depths. It shows the stresses generated in the pile head (both compressive and tensile) due to the impact of the ram at the analyzed depths. It also shows the amount of energy transferred (ENTHRU) to the pile from the hammer at the analyzed depths and the corresponding stroke length of the ram.

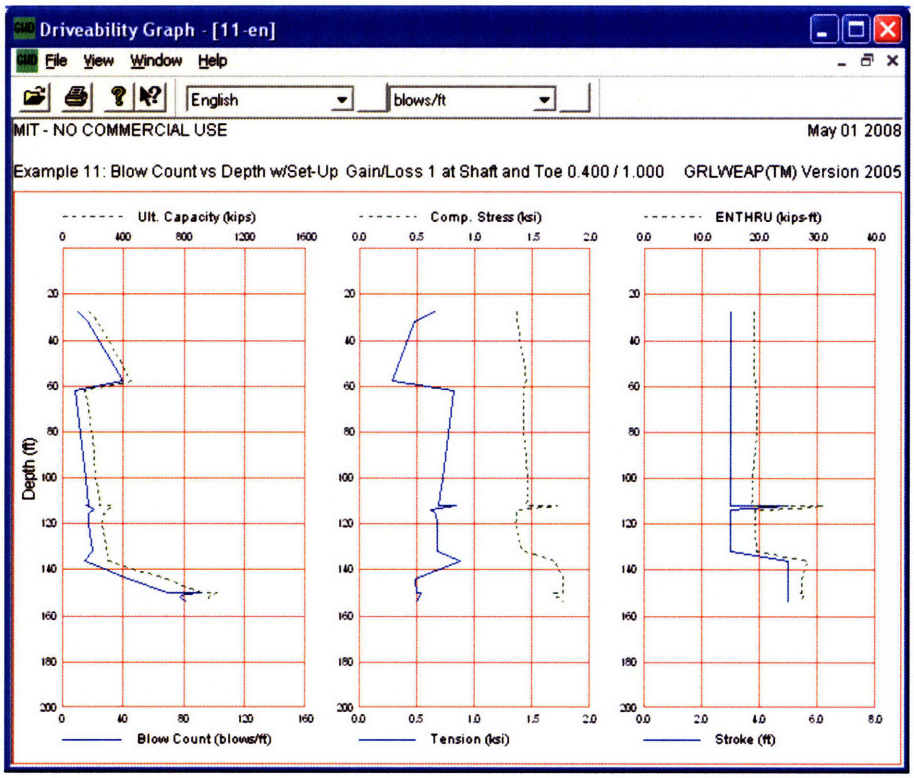

Figure 3.3 A typical driveability graph from GRLWEAP

GRLWEAP Output

Variables such as displacements velocities, accelerations, forces and stresses are calculated for all the pile segments and some hammer segments during the wave equation analysis. Depending upon the user choice, some of those values can be stored during the analysis on the disk. These stored values can be displayed either graphically or numerically in the output. There is an option of Numerical Results which contains an echo print of the input data, driving system, pile model, program performance messages and analysis results, which is useful for checking all the assumptions made.

3.5 Example Problem

A load of form shown in Figure 3.4a is applied on a pile driven into soil with properties summarized in Table 3.1(Simons and Randolph, 1984). The displacement of the pile head is monitored over a period of time by which the induced wave returns to the pile head after reflection at the tip.

Table 3.2 Pile and soil properties in the example problem (Simons and Randolph, 1984)

Pile	Soil
Outer Radius = 0.75 m	Shear Modulus = 10 MPa
Inner Radius = 0.68 m	Density = 2100 kg/m^3
End Condition: Closed	Poisson's Ratio = 0.48
Embedded Length = 30 m	Skin Friction = 100 kPa
Young's Modulus = 210 kN/mm^2	Base Resistance = 900 kPa
Density = 7750 kg/m^3	
Poisson's Ratio = 0.3	

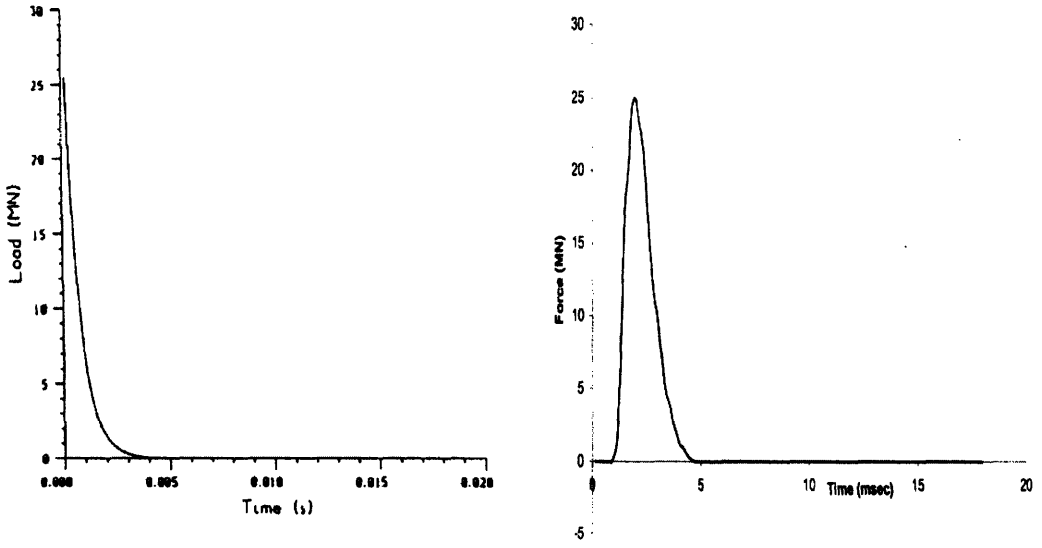

(a) Applied Loading (Simons & Randolph, 1984) (b) Applied Loading in GRLWEAP

Figure 3.4 Load applied on the pile

The loading applied in GRLWEAP starts at an approximate time 0.001 s. The reason for this delay is not known, it might be attributed to the ignition time of the hammer. The peak value of this force is close to 25 MN in both the cases. Simons and Randolph (1984) used three different approaches to solve this problem of pile driving. Two of the methods adopted were that of finite elements and Smith (1960). The third method was a new analytical approach (Simons and Randolph, 1984), based on the work of Novak et al. (1978) and is discussed in Section 3.2. Table 3.3 shows the Smith (1960) parameters used in the problem.

Table 3.3 Smith (1960) parameters used in the example problem

Smith (1960) Parameters	Quake (mm)	Damping (s/m)
Side	2.54	0.164
Base	2.54	0.492

Figure 3.5 compares the results obtained from the three different approaches. The spurious oscillations that are observed in the solution by finite element method, is due to its high frequency dispersion characteristic (Simons and Randolph, 1984). The phenomenon of dispersion gives rise to different wave propagation velocities in the discrete system for different frequencies. The errors due to dispersion add up with time and hence, only short term responses are reliable. Smith (1960) approach does not represent the radiation of wave energy into the soil medium and hence differs from Simons & Randolph (1984) solution. The small difference between Figure 3.5c and 3.5d may be due to the small difference in the loading or the hammers used (no information is available about the type of hammer used for solution represented by Figure 3.5c)

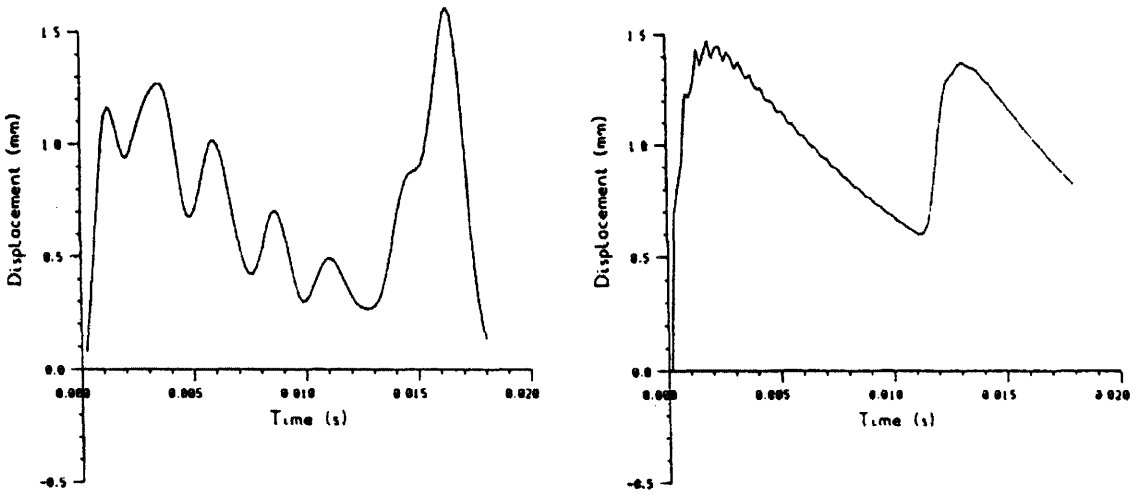

(a) Response using Finite Element Method (b) Response using Simons&Randolph (1984)

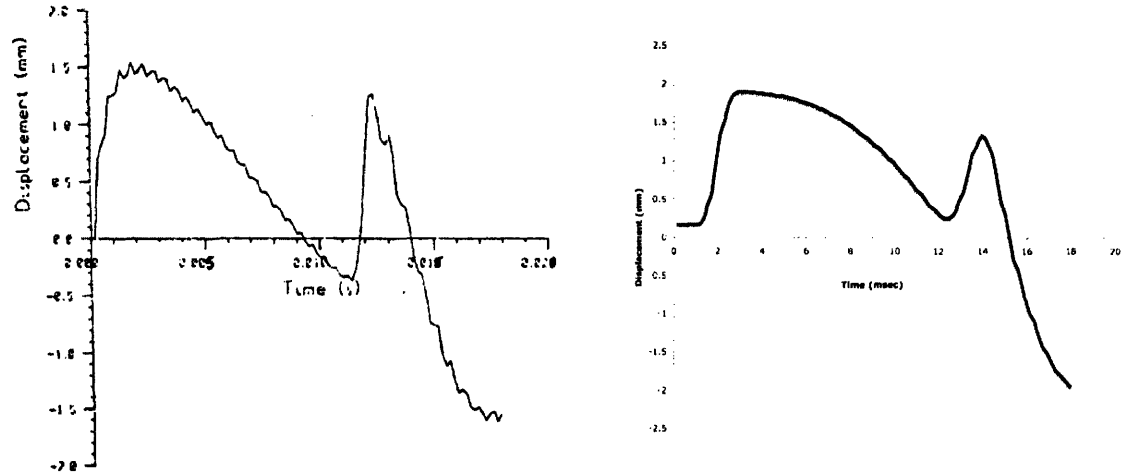

(c) Response using Smith (1960) approach calculated by Simons & Randolph (1984)

(d) Response using Smith (1960) calculated by GRLWEAP

Figure 3.5 Comparison of results from different methodologies

4. Example Analysis

4.1 Introduction

In order to illustrate the design of a pile for an offshore floating wind farm, the Author will focus on a 'typical' soil profile[+]. The site conditions are based on the data published by Jardine (1985) for the well-documented Magnus project in the North Sea. Figure 4.1 shows the 'typical' soil profile. The soil profile is divided into five geotechnical units, based on contractors' reports and fabric studies (Jardine, 1985). Unit I consists of stiff to very stiff clay, which may have been deposited as a lodgement till and consolidated by wave action. This is underlain by a layer of dense to very dense fine sand (up to 3 m thick). Uints II to V are believed to be of glaciomarine origin with some thin lenses of interglacial fine silty sand at approximately 14 m and 19 m depth, which were not thought to have a significant bearing on foundation behavior. Table 4.1 summarizes index properties of the soil. Unit I is slightly leaner and coarser-grained than the deeper layers (Jardine, 1985). It is also has a low compressibility and exists in a very dense and overconsolidated state, which is thought to be due to wave compaction, rather than mechanical overconsolidation (Hight 1983, Jardine 1985). Yield Stress Ratios (YSR – equivalent to apparent OCR) for the top stratum fall between 15 and 25. Strata III to V are relatively more plastic and only lightly overconsolidated with YSR $\approx$ 1.0 at 70 m depth. Stratum II is a transition between stratum I and other lower strata with intermediate properties (YSR falls from $\approx$ 6 at 20 m to $\approx$ 2 at 40 m depth). Figure 4.2

[+] The site is chosen to be typical of continental slope conditions in the Northeastern US.

shows the undrained shear strength profile of the soil, which was obtained by conducting standard UU triaxial tests on 38mm diameter specimens, and OCR and σ'_{v0} profile.

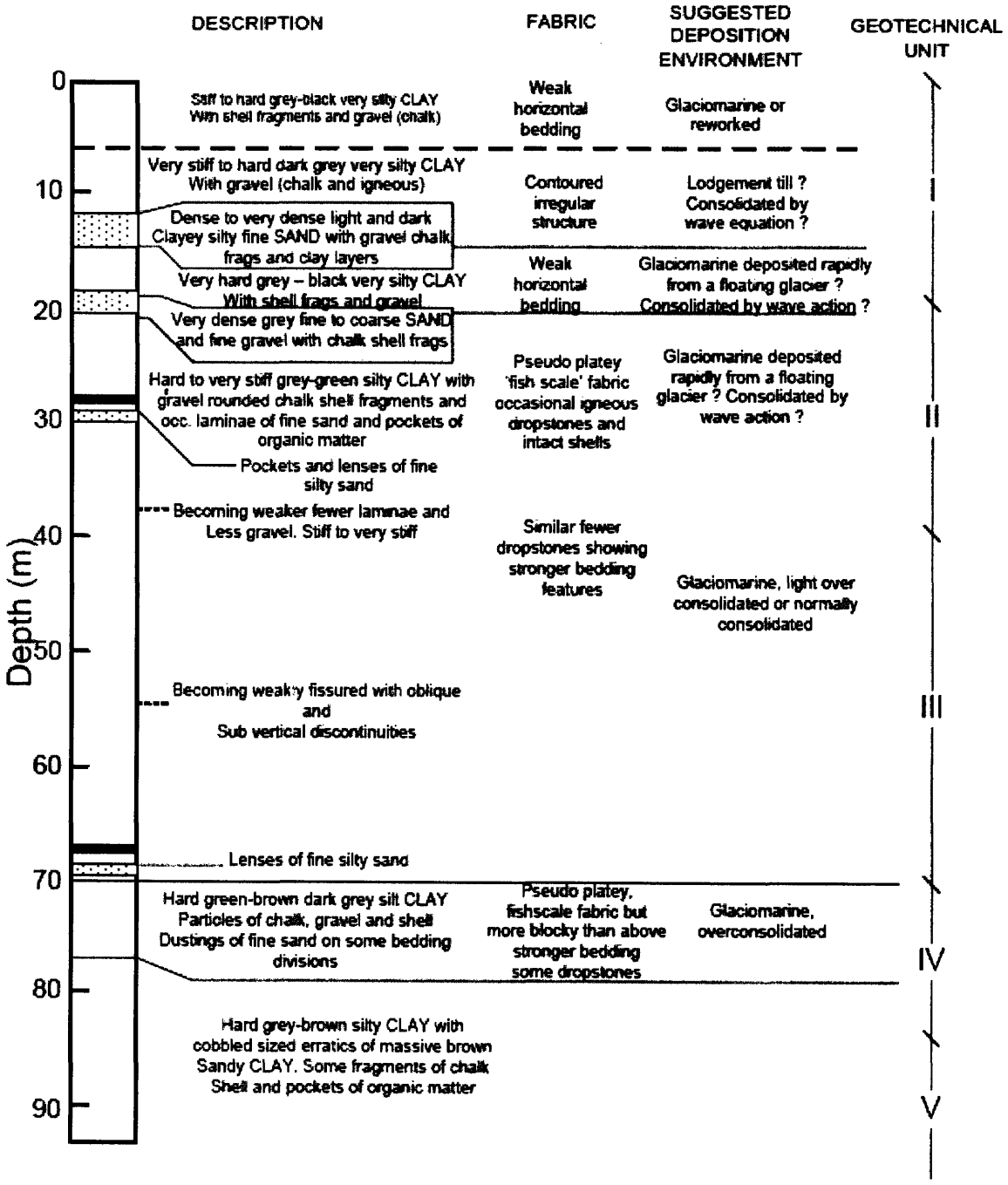

Figure 4.1 Magnus Soil Profile (Jardine, 1985)

Table 4.1 Mean index properties of soil (Jardine and Potts, 1992)

Note: C_c and e_1 apply to the range 2MPa< σ'_v <3MPa, e_1 is void ratio projected for σ'_v = 1kPa

Unit	Depth range below mudline (m)	w (%)	γ_t (kN/m^3)	I_p %	I_L	Oedometer parameters e_1	C_c	% clay
I	0-20	14-20	21.8	17	0.07	0.75	0.12	23.00
II	20-40	16-21	21.1	19	0.09	0.95	0.15	27.00
III	40-70	21-24	20.5	22	0.16	1.25	0.23	34.00
IV	70-84	18-23	20.9	25	0.10	1.10	0.20	34.00
V	below 84	18-21	20.9	24	0.03	1.00	0.16	32.00

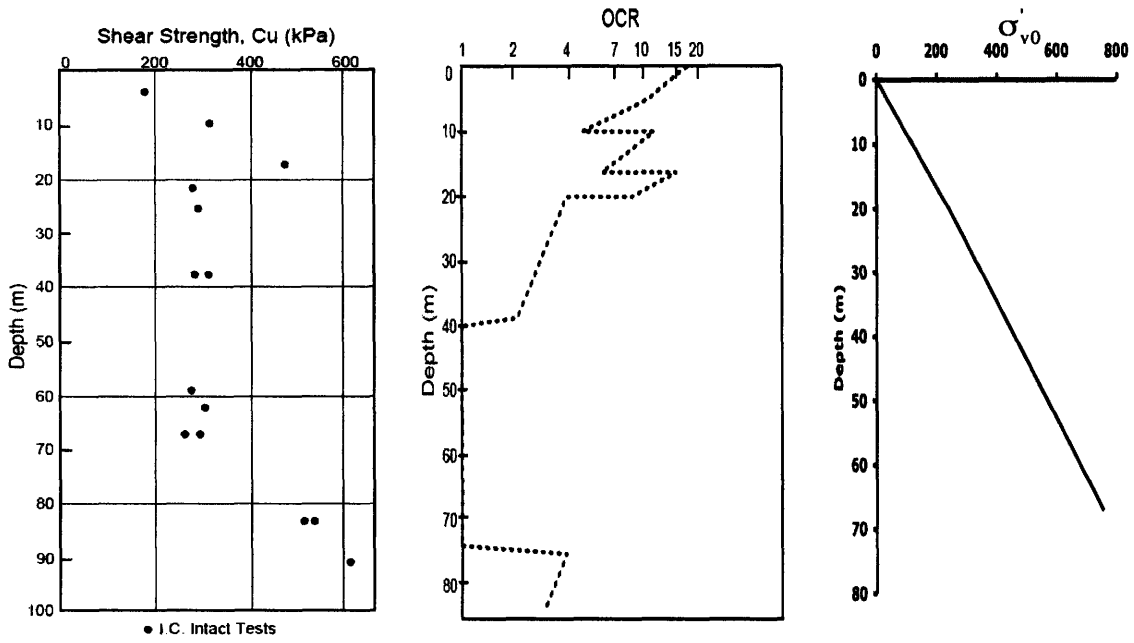

Figure 4.2 Undrained shear strength, OCR and σ'_{v0} profile (Jardine and Potts, 1992)

4.2 Design Loads

Each floating wind turbine will be tethered down to the seabed by four cables each carrying a maximum tension of 783 Tonnes (Tracy, 2007) and imposing an equal amount

of vertical uplift force on the driven piles, which the cable is attached to. Considering a factor of safety of 3, the design load for the pile is 2350 Tonnes (also see Chapter 1 for design constants and structural properties of the platform). All of this force has to be carried by the pile foundations through shaft friction, using either a single monopile or a pile group with a cap template.

4.3 Unit Shaft Resistance (f_s) and Unit End Bearing Resistance (q_{bf})

The pile driving analysis (using GRLWEAP) requires input parameters for the unit shaft friction (f_s) and end bearing resistance (q_{bf}) through the soil profile. Shaft friction between pile and clay layers has been calculated using the method proposed by Randolph and Murphy (1985), which forms the basis of current API code for design of offshore friction piles in clay (see Figure 4.3). The method of Poulos and Davis (1980) has been used to calculate shaft friction in sand (see Figure 4.4). Due to lack of data on engineering properties of the sand layer, some assumptions have been made. The layer between 12-15 m depth is found to be dense to very dense fine sand (Figure 4.1) with estimated relative density, D_r = 60-80% (Vesic, 1977), and estimated friction angle, $\Phi' = 36^0$ based on correlations between Φ', D_r and sand gradation suggested by Schmertmann (1978). Similarly, the sand layer between 20-22 m depth is found to be very dense fine to coarse sand, and $\Phi' = 38^0$ is chosen.

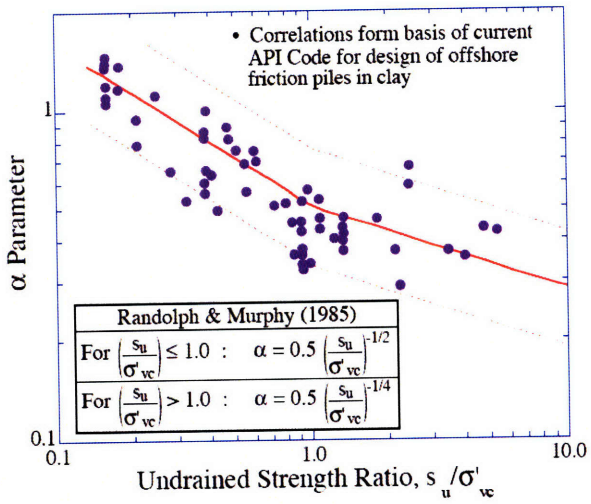

Figure 4.3 Method to calculate shaft friction in clays (Randolph and Murphy, 1985)

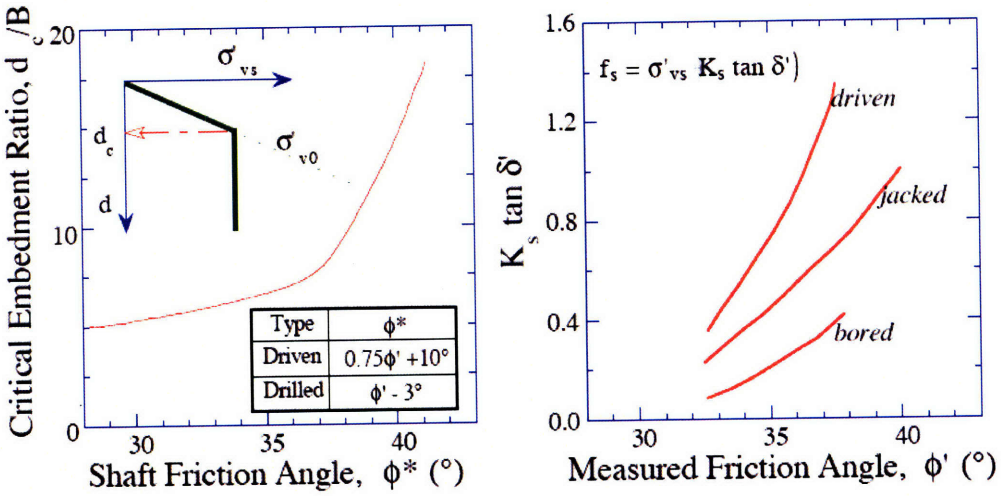

Figure 4.4 Procedure for computing shaft friction of piles in sand

(Poulos and Davis, 1980)

Information on the tip resistance is needed for analyzing pile driving, although it does not contribute to anchor capacity. Tip resistance in sands has been calculated using the empirical results of Vesic (1977) as shown in Table 4.2. N_q values for driven piles are higher than that of drilled shafts due to the compaction of soil below tip during driving

process. It can be observed that there is a range of N_q values for different densities of sand and for calculations, and the lower value of the respective range has been chosen.

Table 4.2 Tip resistance factor, $N_q = q'_{bf} / \sigma'_{v0}$ for piles in sands (Vesic, 1977)

		N_q Values	
Sand Compactness	Relative Density, D_r (%)	Driven Piles	Drilled Shafts
Very Dense	> 80	60 - 200	40 - 80
Dense	60 - 80	40 - 80	20 - 40
Medium	40 - 60	25 - 60	10 - 30
Loose	< 40	20 - 30	5 - 15

Tip resistance in clays has been calculated by using Skempton's (1951) bearing capacity factors.

$$q_b = N_c s_u + \sigma_{v0} \tag{4.1}$$

Where:

q_b = resistance at the tip of the pile;

N_c = Skempton's bearing capacity factor;

s_u = undrained shear strength of the clay representing average strength of soil in zone up to 2B below tip of the pile where B is the diameter of the pile;

σ_{v0} = total vertical stress.

It is recommended to use N_c = 9 for all piles as it is a very good estimate based on empirical results (see Figure 4.5).

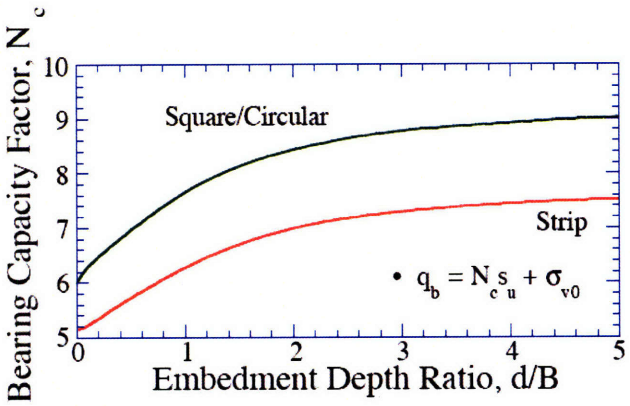

Figure 4.5 Skempton's Method (1951)

4.4 Pile Setup in Soils

Pile setup refers to the increase in shaft capacity of the pile after driving. For clays, setup occurs primarily due to dissipation of excess pore water pressures that are generated during the pile driving process (and the corresponding increase in effective stress acting on the pile shaft). It is very important to estimate the time required for setup, as this affects the scheduling /time delay for hookup of the floating wind turbine, following pile installation. A lot of research has been done to make reliable predictions of setup to offshore piles (Randolph et al., 1977; Whittle, 1992). All the methods assume that the capacity of the driven piles is mainly a function of the changes in effective stresses and soil properties that occur during and post driving.

The concept of pile setup was corroborated and presented with a better formulation by Whittle and Sutabutr (1999) based on strain path method in combination with MIT-E3 effective stress soil model (Whittle, 1987) and non-linear finite element methods. It takes

into account the effects of change in stresses, equivalent pile radius and permeability of the soil to determine the setup parameters (see Figure 4.6). It is based on test data from Boston Blue Clay (BBC) at the Saugus test site and Imperial College Instrumented Pile at Bothkennar site and only valid for lightly overconsolidated soils.

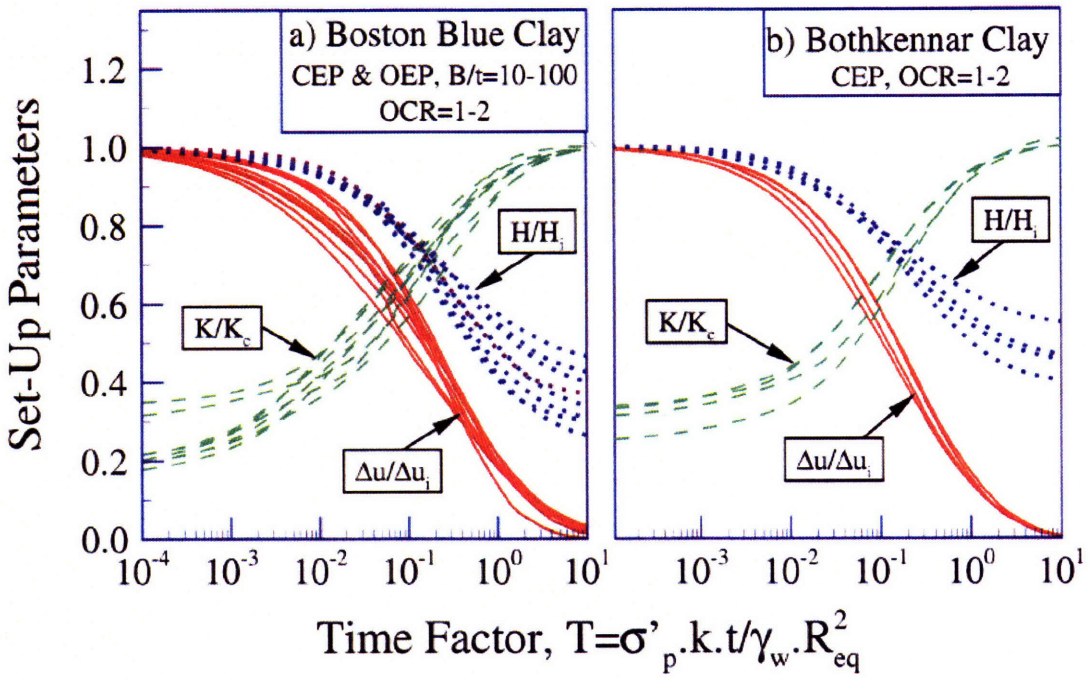

Figure 4.6 Prediction of dimensionless setup factor for soft clays

(Whittle and Sutabutr, 1999)

Instrumented pile loading tests conducted on highly overconsolidated London clay (Bond and Jardine, 1993) show that there is only a slight change in the radial effective stresses during pile loading. They also show that the radial effective stresses decreased during loading in compression and remained almost constant during loading in tension. And the effective stress paths followed by the soil elements close to pile shaft formed a consistent pattern independent of the rate of pile installation. There was no significant change in

capacity of the piles installed in high OCR London clay with time (see Figure 4.7). Since the soil profile considered for the design of piles has top 10-15 m thick layer of high OCR clay (see Figure 4.2), the observations of Bond and Jardine (1993) are very important for prediction of setup time in the selected soil profile.

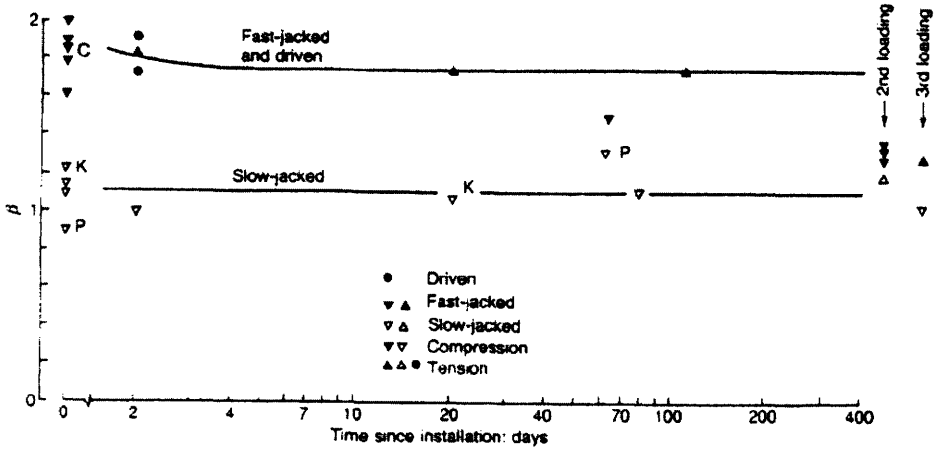

Figure 4.7 Variation in $\beta = f_s/(\sigma_{v0}')_{av}$ with time (Bond and Jardine, 1993)

The presence of sand layers in the soil profile raises questions about pile setup in sands. Chow et al (1996) conducted tests on strain-gauged pipe piles in dense sand at Dunkirk, northern France to study the effects of setup on pile capacity. The results of the tests show that the open-ended steel piles driven into dense marine sand at Dunkirk developed an 85% increase in the shaft capacity in a time of six months to five years after pile installation. Figure 4.8 shows that an increase of 50% in shaft capacity was observed per log cycle of time, once approximately 24 hours have elapsed after driving. One of the possible explanations for this observation is the increase in radial effective stresses, due to reduction of arching effects around the pile, caused by creep in the sand. Strong

dilation during shearing and large increases in radial effective stresses during pile loading due to ageing of the soils can be another possible reason.

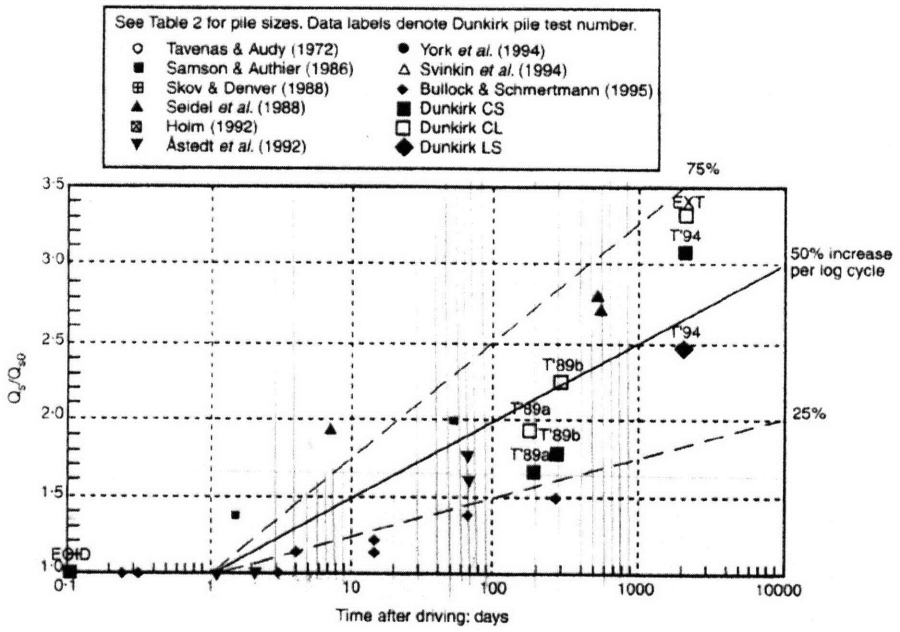

Figure 4.8 Change in shaft capacity with time (Chow et al, 1996)

4.5 Input Parameters

Figure 4.9 shows the unit shaft resistance (f_s) and end bearing resistance (q_{bf}) of soil profile derived from methods mentioned in Section 4.2. Table 4.3 summarizes the input parameters used for GRLWEAP analysis. The soil quake values and damping coefficients have been calculated on the basis of Table 3.1. It has been assumed that there is no soil plug formation during driving.

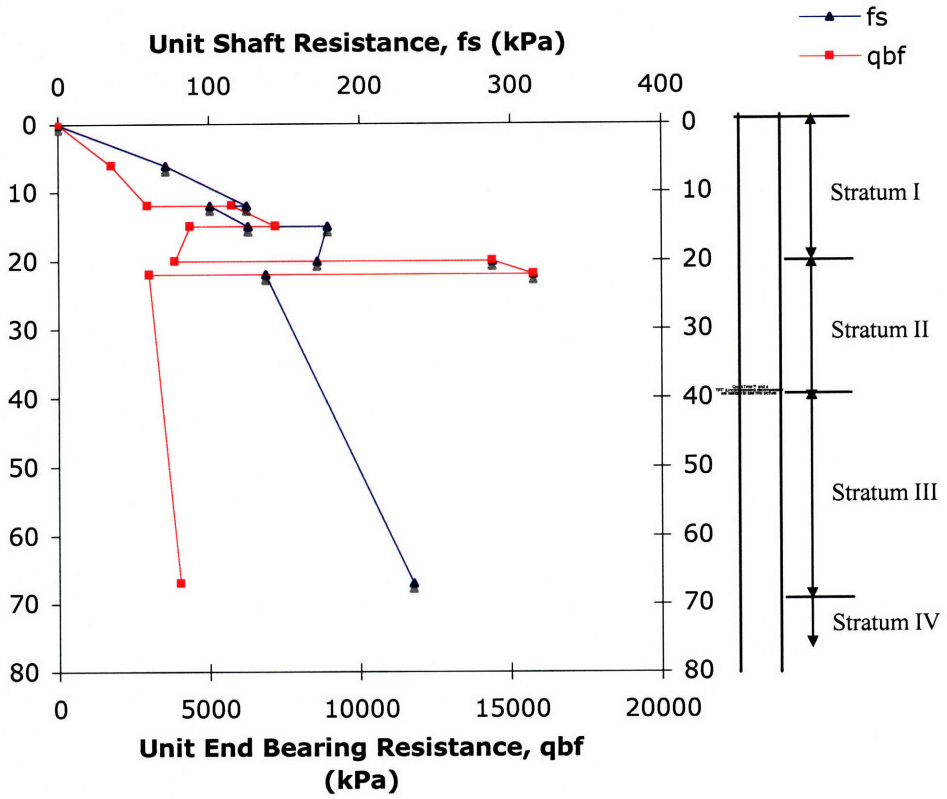

Figure 4.9 Toe resistance and shaft resistance profile of the soil

Table 4.3 Input parameters for example analysis

Depth m	Unit Shaft Resist, f kPa	Unit Toe Resist,q kPa	Skin Quake mm	Toe Quake mm	Skin Damping s/m	Toe Damping s/m
0	0	0	2.5	6	0.656	0.49
6	71.5	1751	2.5	6	0.656	0.49
12	124.8	2962	2.5	6	0.656	0.49
12	100.7	5755	2.5	3	0.164	0.49
15	125.9	7194	2.5	3	0.164	0.49
15	178.7	4377	2.5	6	0.656	0.49
20	171.8	3856	2.5	6	0.656	0.49
20	287.8	14388	2.5	3	0.164	0.49
22	314.9	15742	2.5	3	0.164	0.49
22	137.8	2998	2.5	6	0.656	0.49
67	235.2	4021	2.5	6	0.656	0.49

4.6 Example of Pile Driving Analysis

The first example considers a 24 m long steel pipe pile with 0.47 m outer radius and 0.025 m wall thickness. The initial analysis considers a hammer with ID 326 (IHC S-280, ECH, ram weight 134 kN, rated energy 278 kJ) from the GRLWEAP library. Results from GRLWEAP analysis, Figure 4.10a, show the variation of blow count and ultimate capacity based on static analysis using unit shaft resistance and unit end bearing resistance input parameters, Figure 4.10a also shows variation of stresses (tensile and compressive) and ENTHRU. The slight increase in the blow count observed at a depth of 12 m and 20 m is due to the presence of the thin sand layers. The tensile stresses generated at depth of 5-11 m are well below allowable tensile stress in steel (f_t = 250MPa). It may be noted that the rated energy of the hammer used here is 278 kJ and is an underwater hammer. The maximum and minimum blow energies of the IHC-280 hammer are 200 kJ and 10 kJ respectively*. The energy transferred (ENTRHU) is very low towards the beginning of the driving process because the elastic limit of the soil is readily exceeded and virtually all of the energy applied at the pile head transfers to the soil. After pile penetration of about 7 m, there is a substantial increase in the ENTHRU reaching a maximum of around 110 kJ (efficiency = 40%). This efficiency is close to mean efficiency of gas hammers on steel piles (49% for single acting hammer and 33 % for double acting hammer, Rausche et al.,1985). It can be observed at the stroke was kept constant at 0.91 m throughout the driving process. Similar results are shown (Figure 4.10b) for a pile with penetration depth of 40 m and hammer ID 328 (IHC S-500, ECH, ram weight 246 kN, rated energy 497 kJ) in GRLWEAP.

* www.ihchh.com (accessed May 21, 2008)

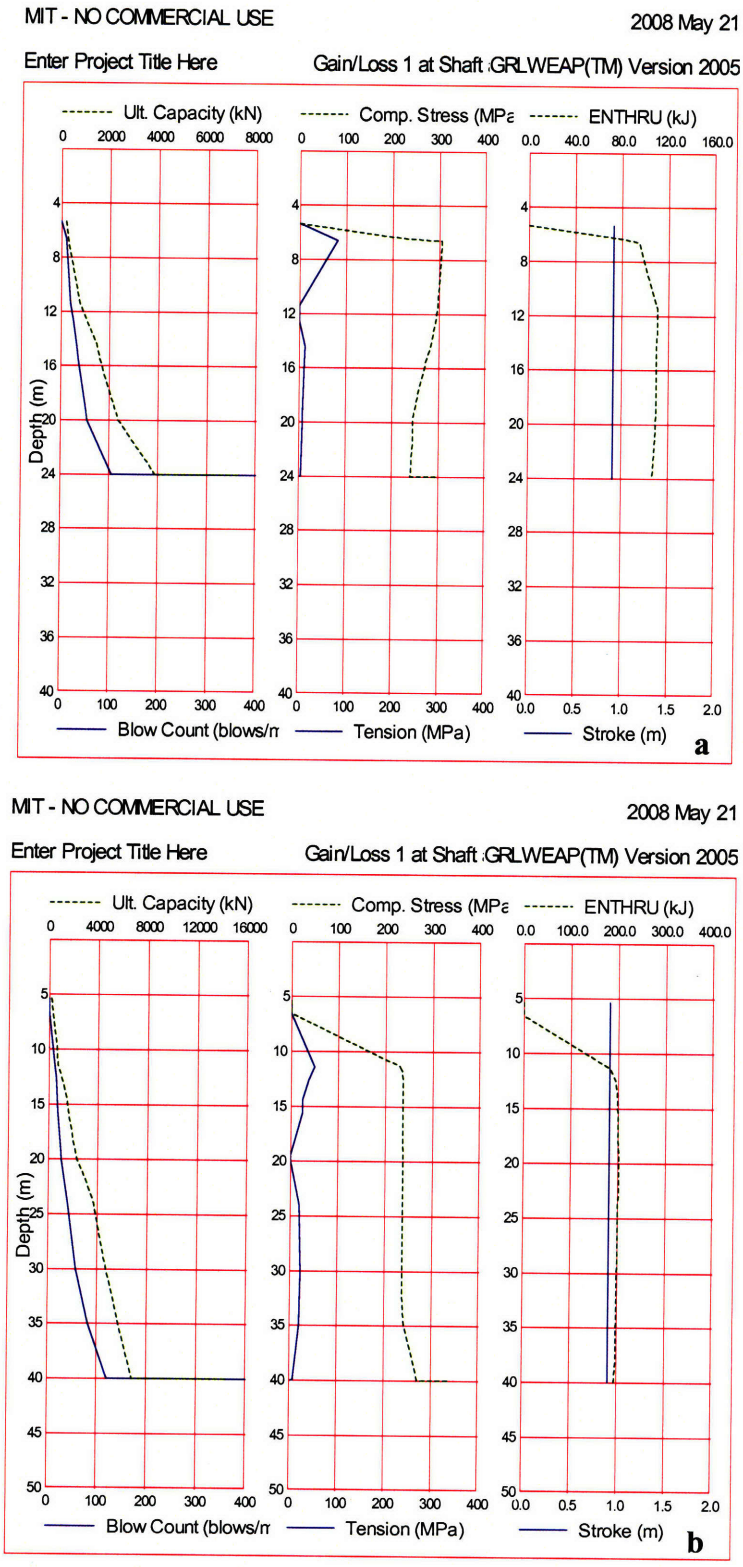

(a) Penetration length, L = 24 (b) Penetration length, L = 40 m

Figure 4.10 Results from GRLWEAP

The total number of blows required for L = 24 m and L = 40 m, N = 740 and 1463, respectively, calculated by GRLWEAP. Assuming a blow rate, 6 blows/min and no interruptions in driving, the total time to drive the piles is 2 hours (L = 24 m) and 4 hours (L = 40 m). Another observation from Figure 4.10 is the increase in ultimate capacity (and blow count) for the last blow. It represents a single strike after complete pile setup has taken place. This re-strike is to check the increase in shaft capacity of the pile with time and can be used to study the pattern of increase in shaft capacities with time through GRLWEAP which assumes a setup time of 1 hour, 1 day and 7 days for sands, fine sands and silts, and clays respectively, the basis of which is unknown to the author. The author has tried to compare the increase in the shaft capacity (and hence total capacity) as suggested by GRLWEAP with MIT-E3 (Whittle and Sutabutr, 1999) predictions for lightly overconsolidated clays in combination with findings of Chow et al. (1996) for sands (50% increase in shaft capacity per log cycle of time). Setup occurs only in sand layers and clay layers below 22 m depth. The upper clay layers are highly overconsolidated and hence, there is no setup in those layers (Bond and Jardine, 1993).

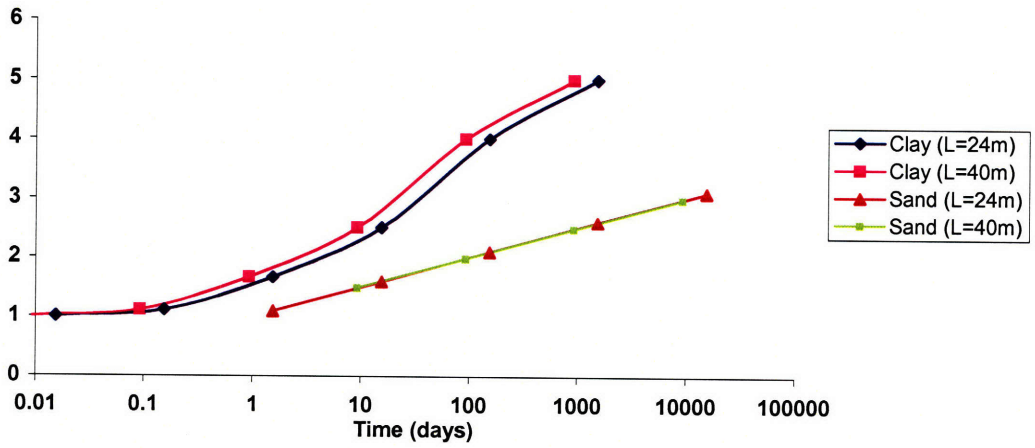

Figure 4.11 Setup factor (vs. time) used in the current analysis

Figure 4.11 shows the variation with time of setup factors for clay layers below 22 m depth and sand layers, derived from methods mentioned above. The setup factor (dimensionless) for clay layer has been calculated at the middle of the layer and assumed to be uniform for the whole layer to simplify calculations. In reality, the setup factor for clay depends on the in-situ preconsolidation pressure (Whittle and Sutabutr, 1999), which varies with depth. Figure 4.12 shows the corresponding increase in the total capacity of the pile. The increase in shaft capacity for L = 24 m comes mainly from sand layers because the clay layer contributing to the setup is only 2 m thick (layer at depth 22-24 m), whereas in the case of L = 40 m, the clay layer contributing to the setup is 18 m thick (layer at depth 22-40 m).

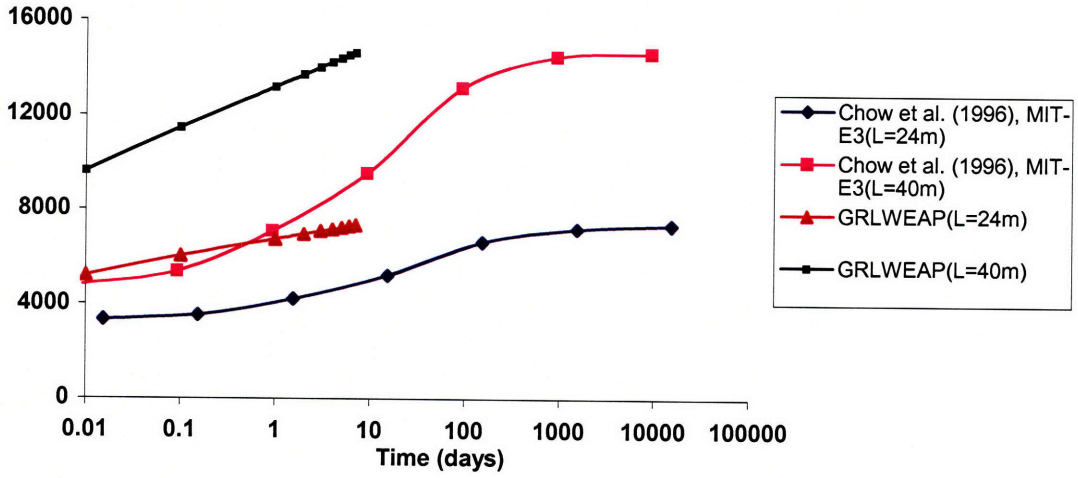

Figure 4.12 Capacity increase as a function of time

GRLWEAP clearly underestimates the pile setup time by a very large amount and the input setup factor and setup time in it should be verified using other reliable approaches discussed above. Since it takes a very long time for complete setup to take place and

turbines will be tethered to the piles much before that, the capacity of the pile depends on the scheduling of the project. Assuming that the turbine is tethered to the piles 10 days after driving the piles, the number of piles required to achieve the design load capacity of 2350 Tonnes for a single tether is shown in Table 4.4.

Table 4.4 Number of piles required for a single tether

Design Load = 2350 Tonnes	L=24 m	L=40 m
Total Capacity (Tones)	500	1000
Tip Resistance (Tonnes)	10.9	14.2
Shaft Capacity (Tonnes)	489.1	985.8
Number of Piles	5	3

The number of piles required to anchor one tether is not only a function of the type and dimensions of the pile, driving assembly, the soil conditions and design load but also the amount of time delay between pile installation and hookup of the wind turbine. It is an optimization problem between all the factors mentioned above to minimize cost of installing an offshore floating wind turbine. One can reduce the number or piles required but at a cost of increased pile length and bigger driving equipments. Setup time also plays an important role because offshore construction costs increase with time.

The ultimate static capacity of 7330.9 kN for L = 24 m calculated by GRLWEAP is compared with that estimated by WEAP based pile driving formulae proposed by Rausche et al. (1985). See Figure 4.13 for pile head force and velocity variation with time.

$$R_d = 0.5(F_0 + Zv_0) + 0.5(F_r - Zv_r) \qquad (4.2)$$

Where:

Z is the pile impedance,

R_d is the dynamic resistance of the pile,

Subscripts 0 and r refer to times t_0 and t_r,

t_0 = time at which the input force (from the hammer) reaches its maximum value

$t_r = t_0 + 2L/c$; time required for the peak force to travel down and back up to the pile head,

F_0 and F_r; v_0 and v_r are the measured forces and velocities at t_0 and t_r, respectively.

Assuming that the dynamic enhancement of soil resistance takes place only at the tip of the pile, the static capacity is estimated from the dynamic resistance. Rausche et al (1985) assumed that the dynamic tip resistance is given by:

$$Q_d = J_c Z v_b \tag{4.3}$$

where J_c is a dimensionless damping coefficient, and v_b is the velocity at the base of the pile. Values of J_c can be backfigured by matching the results of static pile load tests, or can be selected based on recommendations given by Rausche et al (1985) shown in Table 4.5. The static capacity of the pile can be estimated in the following way:

$$R_{st} = 0.5(1 - J_c)(F_0 + Zv_0) + 0.5(1 + J_c)(F_r - Zv_r) \tag{4.4}$$

Table 4.5 Recommended values of J_c (Rausche et al, 1985)

Bearing Layer	Suggested J_c
Sand	0.05 – 0.20
Silty Sand	0.15 – 0.30
Silt	0.20 – 0.45
Silty Clay	0.40 – 0.70
Clay	0.60 – 1.10

Figure 4.13 shows the variation of force (Top F) and velocity (Top V) on the pile head.

Using this methodology, $R_d = 7633$ kN and $R_{st} = \begin{cases} 5590 \text{ kN(for } J_c = 0.6) \\ 1775 \text{ kN(for } J_c = 0.6) \end{cases}$

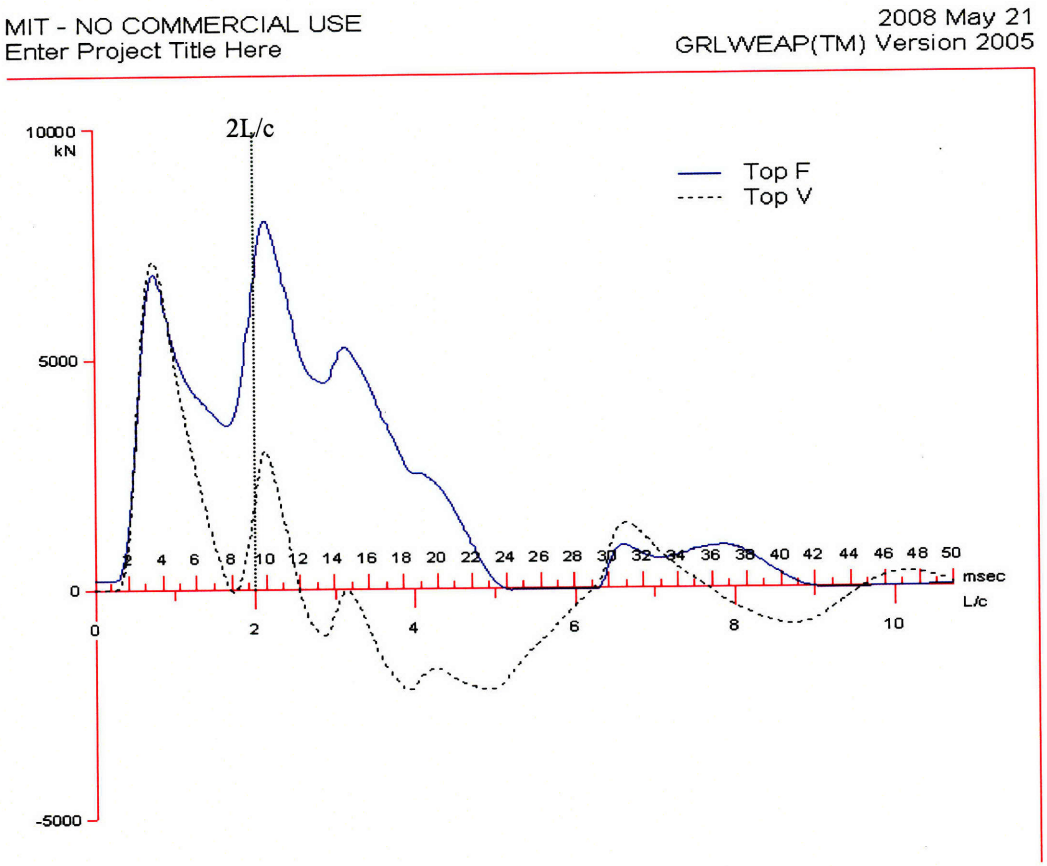

Figure 4.13 Pile head force and velocity variation with time

5. Conclusions

The following conclusions can be drawn from the example analysis of driven pipe piles for offshore floating wind farm:

- There is a considerable increase in shaft capacity of piles in sands and clays (except in highly overconsolidated clays). It becomes an important consideration while scheduling a project and/or estimating costs of the project.

- Larger piles required bigger driving assembly and hence increase costs. But they achieve higher capacity and can cut costs by reducing the number of piles required for the design load. Hence it needs an optimized selection of pile size, driving equipment and delay time between pile installation and tethering of the floating turbine.

- Wave equation analysis is an effective tool to estimate pile capacity and the required driving assembly. It allows the user to try many different pile sizes and driving equipment (hammer, etc.) before actually using one to install the piles.

References

1. API RP 2A (1987) Planning, Designing and Constructing Fixed Offshore Platforms
2. Bond A.J. and Jardine R.J. (1993) "Shaft capacity of displacement piles in a high OCR clay", Geotechnique, Vol. 45, No. 1, pp. 3-23
3. Chow F.C., Jardine R.J., Nauroy J.F. and Brucy F. (1997) "Time-related increases in the shaft capacities of driven piles in sand", Geotechnique, Vol. 47, No. 2, pp. 353-361
4. Chow Y.K., Karunaratne G.P., Wong K.Y. and Lee S.L. (1987) "Prediction of load-carrying capacity of driven piles", Canadian Geotechnical Journal, Vol. 25, pp 13-23
5. Chow Y.K. and Smith I.M. (1984) "A numerical model for the analysis of pile driveability", 2nd Intl. conference on Application of Stress-Wave Theory to Piles, Stockholm
6. Chow Y.K., Wong K.Y., Karunaratne G.P. and Lee S.L. (1988) "Wave equation analysis of piles – A rational theoretical approach", 3rd Intl. conference on Application of Stress-Wave Theory to Piles, Canada
7. Ciamberlano F., Nitschke J., Kragelund N., Thiede J., Fusselbaugh M., Johst M. and Velde F. (2006) "Engineering Insurance of Offshore Wind Turbines", 39th IMIA Annual Conference of The International Association of Engineers Insurers, September 12, Boston

8. Corte J.F. and Lepert P. (1986) "Résistance latérale pendant le battage et l'essai dynamique des pieux" In C.R. 3° Colloque International sur les méthodes numériques de calcul des pieux pour les ouvrages en mer, Nantes, éd. Technip, Paris, pp. 19-33
9. Dyminsky A.S., Parente-Ribeiro E., Romanel C. and Beim J.W. (2000) "Pile capacity prediction using neural networks technique", Proceedings of the 6th International Conference on the Application of Stress-Wave Theory to Piles, Rotterdam
10. Gerwick B.C. (2007) "Construction of Marine and Offshore Structures", Third edition, CRC Press
11. Goble G.G. and Rausche F. (1976) "Wave equation analysis of pile driving – WEAP program", Federal Highway Administration, Vol. 1-4, Report No. FHWA-IP-76-14.1-14.4
12. Goble Rausche Likins and Associates (1999) *GRLWEAP Wave Equation Manual*; Cleveland, Ohio
13. Harrison R., Hau E. and Snel H. (2000) "Large Wind Turbines-Design and Economics", John Wiley & Sons
14. Heerema, E.P. (1979) "Relationship between Wall Friction, Displacement Velocity and Horizontal Stress in Clay and Sand for Pile Driveability Analysis," Ground Engineering, Vol. 12, No. 1, pp. 55-65
15. Hight D.W. (1983) "Laboratory Investigations of sea bed clays", PhD Thesis, University of London, Imperial College

16. Isaacs D.V. (1931) "Reinforced concrete pile formula", Journal of the Institution of Engineers Australia, Vol. 12

17. Isben L. (2005) "Bucket foundation, a Status", Conference Proceedings Copenhagen Offshore Wind, 26-28 October, Copenhagen, DK

18. Jardine R.J. (1985) "Investigations of pile-soil behavior, with special reference to the foundations of offshore structures", PhD Thesis, University of London, Imperial College

19. Jardine R.J. and Potts D.M. (1992) "Magnus Foundations: Soil properties and predictions of field behavior", Proceedings of the Conference Recent large-scale pile tests in clay, 23-23 June, London

20. Jonkman J. M. and Sclavounos P. D., (2006) "Development of Fully Coupled Aeroelastic and Hydrodynamic Models for Offshore Wind Turbines", ASME Wind Energy Symposium, Reno, Nevada

21. Kuhn M., Bierbooms W.A.A.M., van Bussel G.J.W., Ferguson M.C., Goransson B., Cockerill T.T., Harrison R., Harland L.A., Vugts J.H. and Wiecherink R., (1998) "Structural and Economic Optimization of Botton-mounted offshore wind energy converters", Institute for Wind Energy, Delft University of Technology, Delft

22. Lee K. H., (2004) " Responses of Floating Wind Turbines to Wind and Wave Equation", Master of Science Thesis, Massachusetts Institute of Technology

23. Lee S.L., Chow Y.K., Karunarathne G.P. and Wong K.Y. (1988) "Rational wave equation model for pile driving analysis" Journal of Geotechnical Engineering ASCE, Vol. 114, N°3.

24. LIC Engineering A/S (2000) Blyth Wind Farm, Northumberland

25. LIC Engineering A/S (2003) North Hoyle Wind Farm, North Wales

26. LIC Engineering A/S (2003) Scroby Sands Wind Farm, England

27. Likins G.E. (1984) "Field measurements and the pile driving analyzer", Proceedings of the 2nd International Conference on the Application of Stress-Wave Theory to Piles, Stockholm

28. Lysmer J. and Richart F.E. (1966) "Dynamic response of footing to vertical loading", Journal of Soil Mechanics and Foundations Division, ASCE, Vol. 92, No. SM1, pp. 65-91

29. Massarsch K.R. (1992) "Static and dynamic soil displacements caused by pile driving", Keynote Lecture, 4th Intl. Conf. on the Application of Stress-Wave Theory to Piles, Netherlands

30. Meyerhof G.G. (1976) "Bearing Capacity and Settlement of Pile Foundations," ASCE JGED, Vol. 102, No. GT3, pp. 197-228.

31. Mukaddam M.A., Iskandarani W.M. and Hussein M. (2000) "Hammer system design using wave equation analysis for testing cast-in-situ concrete piles", Proceedings of the 6th International Conference on the Application of Stress-Wave Theory to Piles, Rotterdam

32. Musial W., Butterfield C. P., (2004) " Future of Offshore Wind Energy in the United States", National Renewable Energy Laboratory, Energy Oceans Proceedings, Palm Beach, FL

33. Musial W., Butterfield S. and Ram B., (2006) "Energy from Offshore Wind", National Renewable Energy Laboratory, Golden CO

34. Nguyen T.T., Berggren B. and Hansbo S. (1988) "A new soil model for pile driving and driveability analysis", 3rd International Conference on Application of Stress-Wave Theory to Piles, Canada

35. Novak M. (1977) "Vertical vibrations of floating piles", Proceedings of the ASCE, Vol. 103, EMI, pp. 153-168

36. Novak M., Nogami T. and Aboul-Ella F. (1978) "Dynamic soil reactions for plane strain case", Journal of Engineering Mechanics Division, ASCE, Vol. 140, No. EM4, pp. 953-959

37. Offshore Wind Energy Workshop on "Structure and Foundations Design of Offshore Wind Installations", March 1, 2000, CLRC Rutherford Appleton Laboratory.

38. Paikowsky S.G. and Chernauskas L.R. (1992) "Energy approach for capacity evaluation of driven piles", Proceedings of the 4th International Conference on the Application of Stress-Wave Theory to Piles, The Netherlands, pp. 595-604

39. Pelleau R., Cochard C., Mondeil L. and Menuier J. (1980) "Instrumentation of offshore piles during driving", International Seminar on the Application of Stress-Wave Theory on Piles, Stockholm

40. Pile Driving Analysis-State of the Art (1969) Report by Texas Transportation Institute, Texas A&M University

41. Poulos, H.G. and Davis, E.H. (1980) "Pile Foundation Analysis and Design", J. Wiley & Sons, New York

42. Presentation by Mohamed A., GE Wind Energy at Deepwater Wind Energy Workshop, Washington D.C., October 26-27, 2004. Website: http://www.energetics.com/deepwater.html

43. Randolph M.F. and Simons H.A. (1986) "An improved soil model for one-dimensional pile driving analysis", Proceedings of the 3rd International Conference on Numerical Methods in Offshore Piling, Nantes, pp. 3-17

44. Rausche F. (2000) "Pile driving equipment: Capabilities and properties", Keynote lecture, Proceedings of the 6th International Conference on the Application of Stress-Wave Theory to Piles, Rotterdam

45. Rausche, F., Likins, G. E., Ren-Kung, S. (1992) "Pile integrity testing and analysis", Proceedings of the 4th International Conference on the Application of Stress-Wave Theory to Piles, Netherlands, pp. 613-617

46. Rausche F., Robinson B. and Seidel J. (2000) "Combining static pile design and dynamic installation analysis in GRLWEAP", Proceedings of the 6th International Conference on the Application of Stress-Wave Theory to Piles, Rotterdam

47. Sakai T. (1988) "Solution of the wave equation for pile-driving analysis", 3rd Intl. conference on Application of Stress-Wave Theory to Piles, Canada

48. Samson C.H. (1962) "Pile driving analysis by the wave equation (computer procedure)", Report of the Texas Transportation Institute, Texas A&M University

49. Simons H.A. and Randolph M.F. (1984) "A new approach to one dimensional pile driving analysis", 5th International Conference on Numerical Methods in Geomechanics, Nagoya

50. Skempton A.W. (1951) "The bearing capacity of clays" Proceedings of the Building and Research Congress, London, Vol. 1, pp.180–189

51. Smith E.A.L. (1960), "Pile Driving Analysis by the Wave Equation", ASCE Journal of the Geotechnical Engineering Division, Vol. 86, pp 35-61

52. Tracy C., (2007) "Parametric Design of Floating Wind Turbines", Master of Science Thesis, Massachusetts Institute of Technology

53. Vesic, A.S. (1977) "Design of Pile Foundations", National Co-operative Highway Research Program, Synthesis of Highway Practice No. 42, Transportation Research Board, NRC, Washington, DC

54. Volund P., (2005) "Concrete is the Future for Offshore Foundations", Proceedings Copenhagen Offshore Wind, 26-28 October, Copenhagen, DK

55. Wind Directions Gravity Foundations (2003) "A Danish – Polish Collaboration", page 28, July/August

56. Wayman E., (2006) "Coupled Dynamics and Economic Analysis of Floating Wind Turbine Systems", Master of Science Thesis, Massachusetts Institute of Technology

57. Wayman E.N., Sclavounos P.D., Butterfield S., Jonkman J. and Musial W. (2006) "Coupled Dynamic Modeling of Floating Wind Turbine Systems", Offshore Technology Conference, May 1-4, Houston, Texas

58. Whittle A.J. (1992) "Assessment of an effective stress analysis for predicting the performance of driven piles in clays," Advances in Underwater Technology, Ocean Science and Offshore Engineering Volume 28, Offshore Site Investigation and Foundation Behaviour, Society for Underwater Technology, London, pp. 607-643

59. Whittle A.J. and Sutabutr T. (1999) "Prediction of pile set-up in clay", Proceedings TRB

60. http://www.offshorewindenergy.org/ (November 9, 2005)

61. http://www.hornsrev.dk/ (January 23, 2006)

62. http://www.offshorewindenergy.org/ (accessed May 17, 2008)

Appendix A

Name of project or study and site	Study (S)/ Project (P) year	No. units x unit capacity (MW)	V_{hub} (m/s)	Distance from shore (km)	Water depth (m)	Specific cost (EUR/kW)	Energy costs[a] (EURcent/kWh)
Phase CII, North Sea, UK	S91	711 x 3	8.3	N.A.	16-21	1900	13
Blekinge, Baltic, SE	S91	98 x 3	9	10	15-20	3000	9.1
Vindeby, Baltic, DK	P91	11 x 0.45	7.5	1.5	3-5	2150	8.5
RES, North Sea, UK	S93	41 x 0.4	7.4	~5	~12	4500	16
Lely, Ijsselmeer, NL	P94	4 x 0.5	7.7	1	5-10	1700	8.3
SK Power, Baltic, DK	S94	180 x 1	8.2	17	8-10	1900	6.7
Tuno, Knob, Baltic, DK	P95	10 x 0.5	~7.5	6	3-5	2200	6.6
Thyssen, Baltic, DE	S95	140 x 1.5	~7.8	4	5-10	1400	6.6
BMFT, Baltic, DE	S95	100 x 1.2	~7.5	~7	~10	1250	5.1
Horns Rev, North Sea, DK	S97	80 x 1.5	9.2	~15	5-11	1650	4.9
Scroby Sands, North Sea, DK	S97	25 x 1.5	~8.2	3	N.A	1150	~4.5
Bockstigen-Valar, Baltic, SE	P97	5 x 0.55	8	4	6	1500	4.9
Nearshore, North Sea, NL	S97	~100 x 1	9	8	13-17	1900	6.4
Opti-OWECS, North Sea, NL	S98	100 x 3	8.4	11.4	14-19	1250	5.1
Middlegrunden	P2000	20 x 2	7.1	2	3-6	1130	5.3

[a]Energy costs for 20 year loan and 5% real interest rate, no inflation, recent exchange rate (2000)

Source: Harrison R., Hau E. and Snel H., (2000) "Large Wind Turbines-Design and Economics", John Wiley & Sons, Ltd.

Appendix B

North Hoyle Wind farm

Type of structure: Wind turbines, 2 MW.

Location: Irish Sea. Liverpool Bay.

Maximum water depth: 21 m

Pile diameter at seabed: 4 m

Soil conditions: 10 m sediments, sand and clay underlain by Mudstone and sandstone.

Year of installation: 2003

Installation method: Driving through upper sediment layers followed by drilling and driving through rock layer.

Number of foundations: 30

Maximum pile penetration below seabed: 33 m

Connection tower/pile: Flange connection on grouted transition piece.

Special feature: Grouted transition piece between pile and tower above sea water level.

Scour protection: Stones placed on stony sea bottom protecting power cables.

Scroby Sands Wind farm

Type of structure: Wind turbines, 2 MW

Location: North Sea, Great Yarmouth.

Maximum water depth: 21 m

Pile diameter at seabed: 4.2 m

Soil conditions: Dense to medium sand.

Year of installation: 2003-2004

Installation method: Driving with hydraulic hammer (IHC 1200)

Number of foundations: 30

Maximum pile penetration below seabed: 31 m

Connection tower/pile: Flange connection.

Special feature: Pile driven with flange (no transition piece).

Scour protection: Stones placed in fully developed scour holes and base of piles.

Blyth Wind farm

Type of structure: Wind turbines, 1.75 MW.

Location: North Sea off Blyth, N of Newcastle.

Maximum water depth: 8-9 m

Pile diameter at seabed: 3.5 m

Soil conditions: Underwater rock outcrop (sandstone, mud stone, coal)

Year of installation: 2000

Installation method: Core drilling and grouting.

Number of foundations: 2

Maximum pile penetration: 12 m and 15 m

Appendix C

Manufacturer: MENCK

- MHU-S hammer series: Can perform under water piling up to 400 m (1,300 ft) water depth
- MHU-T hammer series: Developed for underwater applications up to 2,000 m (6,500 ft) water depth

Manufacturer: IHC

- S-35, S-70, S-90, S-280 and S-500

Appendix D

Parametric Study

A 45 ton design-load pile is to be driven through a loose non-cohesive layer into a dense, coarse sand with gravel. (Example 1 in GRLWEAP Manual, 2005)

Pile: HP 12x53, 40 ft (12.2 m) in length

Table D.1 Effect of cushion stiffness on maximum force on pile head

Ru (kips)	30	60	120
Stiffness (kip/in)	Max Force on pile head (kips)	Max Force on pile head (kips)	Max Force on pile head (kips)
540	218	222.6	227.9
1080	253.7	259.3	267.9
2700	307.9	312.6	316.6
27000	433.4	438	442.9

Table D.2 Effect of cushion stiffness on maximum displacement of pile head

Ru (kips)	30	60	120
Stiffness (kip/in)	Max Disp of pile head (in)	Max Disp of pile head (in)	Max Disp of pile head (in)
540	4.245	1.918	0.892
1080	4.271	1.94	0.929
2700	4.278	1.95	0.959
27000	4.249	1.943	0.975

Increasing cushion stiffness increases maximum force and hence stress in the pile head. Increasing cushion stiffness has a little effect on maximum displacement of pile head. From Table D.1 and D.2, we can observe that increasing cushion stiffness to increase the rate of penetration is not a good idea because it increases the stresses in the pile without much efficiency and can damage the pile particularly in the case of concrete piles.

Table D.3 Effect of Coefficient of Restitution (COR) on maximum displacement of pile head (stiffness of cushion kept constant at 540 kip/in)

Ru (kips)	30	60	120
COR	Max Disp (in)	Max Disp (in)	Max Disp (in)
0.2	3.909	1.711	0.742
0.5	4.025	1.784	0.81
0.8	4.245	1.918	0.892

With increase in COR, the amount of energy transferred to the pile from the hammer increases and hence the displacement of the pile head increases. Therefore, increasing COR of cushion material is a much better option to increase the rate of penetration than increasing its stiffness.

Table D.4 Effect of breaking hammer into smaller segments for WEAP analysis when no cushion is used (stroke = 2.7 ft)

Length of hammer (in)	104.41	48
No. of segments of Hammer	Maximum Compressive Stress (kip/in^2)	Maximum Compressive Stress (kip/in^2)
2	10.5	10.76
5	10.8	11.06
8	10.88	11.13
10	10.92	11.19
No. of segments of Hammer	Maximum Tensile Stress (kip/in^2)	Maximum Tensile Stress (kip/in^2)
2	0.13	0.16
5	0.18	0.2
8	0.19	0.21
10	0.19	0.21
No. of segments of Hammer	Max Disp of Pile Head (in)	Max Disp of Pile Head (in)
2	1.895	1.882
5	1.888	1.876
8	1.886	1.874
10	1.886	1.874

Smith suggested use a single weight for a hammer because it is generally short and rigid. But from Table D.4 we can see that there is a remarkable change in WEAP solution even for a short hammer. This is the case when no cushion is used.

Table D.5 Effect of breaking hammer into smaller segments for WEAP analysis when cushion is used (stroke = 2.7 ft)

Length of hammer (in)	104.41	48
No. of segments of Hammer	Maximum Compressive Stress (kip/in^2)	Maximum Compressive Stress (kip/in^2)
2	7.71	7.46
5	7.66	7.54
8	7.65	7.57
10	7.66	7.6
No. of segments of Hammer	Maximum Tensile Stress (kip/in^2)	Maximum Tensile Stress (kip/in^2)
2	0.17	0.17
5	0.18	0.18
8	0.19	0.18
10	0.19	0.19
No. of segments of Hammer	Max Disp of Pile Head (in)	Max Disp of Pile Head (in)
2	1.924	1.906
5	1.916	1.902
8	1.914	1.902
10	1.914	1.903

From Table D.5 we can observe that the change in WEAP solution when a hammer is divided into smaller segments is not much when a cushion is used as compared to the case presented in Table D.4 where there was no cushion and involved a direct steel to steel impact. This occurs because it is difficult to put a spring with appropriate stiffness between hammer and anvil, which can depend on elasticity of anvil and/or hammer. Hence, it is advisable to divide ram into smaller segments for a better WEAP solution.